NESTORE algorithm: a machine learning approach for strong aftershock forecasting. Comparison of California, Italy, Western Slovenia, Greece and Japan results

S. Gentili[1*], P. Brondi[1], G. D. Chiappetta[1], G. Petrillo[2], J. Zhuang[3], E.-A. Anyfadi[4],F. Vallianatos[4], L. Caravella[1], E. Magrin[1], P. Comelli[1], R. Di Giovambattista[5]

1. National Institute of Oceanography and Applied Geophysics - OGS, Via Treviso 55, 33100 Udine, Italy; sgentili@ogs.it, pbrondi@ogs.it, gchiappetta@ogs.it, lcaravella@ogs.it, emagrin@ogs.it, pcomelli@ogs.it
2. Earth Observatory of Singapore (EOS), Nanyang Technological University (NTU), 50 Nanyang Avenue, Singapore 639798; giuseppe.petrillo@ntu.edu.sg
3. The Institute of Statistical Mathematics – ISM, 10-3 Midori-cho, Tachikawa Tokyo 190-8562, Japan; zhuangjc@ism.ac.jp
4. Section of Geophysics-Geothermics, Department of Geology and Geoenvironment, National and Kapodistrian University of Athens, 15784 Athens, Greece; elenanif1305@gmail.com, fvallian@geol.uoa.gr
5. Istituto Nazionale Di Geofisica E Vulcanologia, Rome, Italy; rita.digiovambattista@ingv.it

corresponding author: Stefania Gentili sgentili@ogs.it

Keywords

Machine learning, cluster identification, strong aftershock, earthquake forecasting, outliers detection.

Abstract

Large earthquakes are often followed by aftershocks, which can cause further damage and cost lives. A pattern recognition approach called NESTORE has been developed to forecast whether one of these subsequent large events is to be expected in an occurring seismicity cluster. This method, which has already been successfully applied in Italy, Slovenia, California, Greece and Japan, has been optimized in the NESTOREv1.0 software written in MATLAB. Using machine learning, NESTOREv1.0 provides a probabilistic forecast of earthquake clusters where a mainshock is followed by a significant aftershock. It classifies clusters as Type A (mainshock and strongest aftershock differ by ≤1 magnitude unit) or Type B (larger difference). NESTOREv1.0 adapts to specific regions through supervised training. It trains one-node decision trees on individual features at increasing time intervals, selects the best classifiers, and combines them using a Bayesian method to forecast Type A clusters. Recent improvements to the algorithm added a new approach for identifying clusters based on ETAS and an innovative method for detecting outliers before training.

This study compares results from Greece, Italy, Western Slovenia, California and Japan, highlighting the performance on independent test sets and seismicity features in different regions and interpreting the differences between regions.

1. Introduction

The increasing availability of high-quality seismic data and the advancement of machine learning techniques applied to seismology (DeVries et al, 2018; Schimmenti et al, 2024; Stockman et al., 2023; Karimzadeh et al., 2019; Zhao et al., 2022; Wang et al., 2019; Liu et al.,2024: Mignan and Broccardo, 2020) have opened new roads for improving aftershock forecasting, a crucial component of seismic hazard assessment. In this context, we developed the NESTORE (NExt STrOng Related Earthquake) algorithm, a data-driven approach designed to identify and classify clusters with strong aftershocks using supervised learning methods. This study presents the outcomes of applying NESTORE in five tectonically diverse regions - California, Italy, Western Slovenia, Greece, and Japan - allowing for a comparative analysis of its performance and generalization capability.

In this paper, we summarize, integrate, and coherently compare the results of previous NESTORE applications, which have been presented individually in papers, conferences, workshops, and theses

(Gentili and Di Giovambattista, 2017, 2020, 2022; Gentili et al., 2023, 2023b; Anyfadi, 2023; Anyfadi et al., 2023; Brondi et al., 2025; Gentili et al., 2024, 2025).

Here, we aim to jointly exploit these results to improve the understanding of feature performance. By comparing the behaviour of features and threshold values in different seismotectonic domains, we seek to identify patterns and evaluate how different tectonic settings may influence predictive capabilities, providing clues for future methodological and operational developments.

As NESTORE is also applied to new clusters, some results are shown here for the first time.
Over the years, the method has been modified and improved to make it more robust and to meet the challenges of analysing new regions. The paper is organised as follows: Section 2 describes the regions where NESTORE has been applied from a seismotectonic perspective, highlighting the differences within and between regions. Section 3 provides a detailed description of the newer version of the method. Section 4 illustrates how the results differ between regions both in terms of the performance of the algorithm and the parameters obtained through training. Finally, Section 5 discusses and interprets the differences observed in the different studied regions, and explores the limitations and advantages of the method, as well as the research approaches we have pursued to address these limitations.

2. Analyzed regions seismotectonic and available data

The NESTORE algorithm has been successfully applied in several regions (see Fig. 1) characterized by different productivity and characteristics of seismic clusters. In the following sections we summarize the seismotectonic regimes of the analyzed regions.

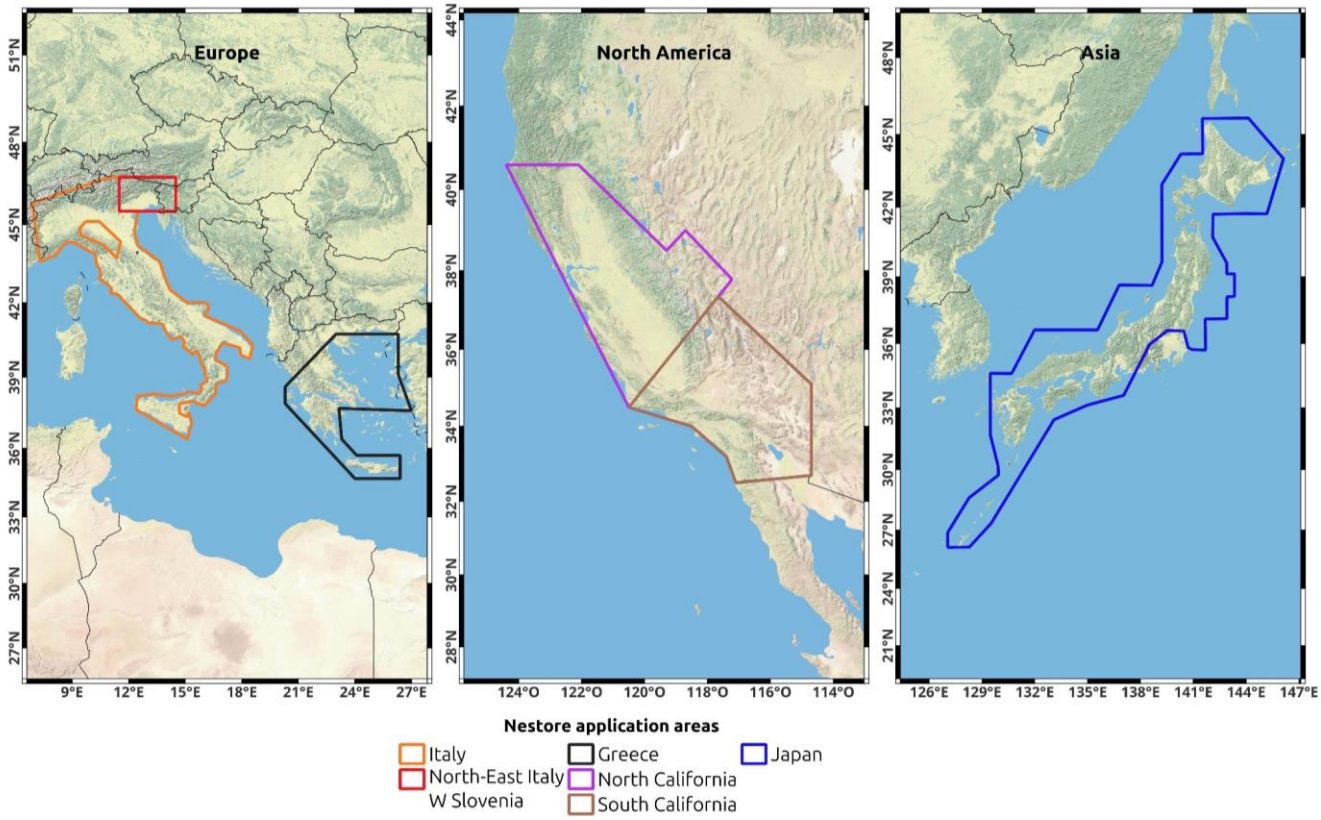

Fig. 1: Analyzed areas in past NESTORE applications

It is important to point out that the quality of NESTORE's performance is highly dependent on the selected area and the quality and consistency of the catalogue. Therefore, we have conducted preliminary analysis of the available catalogues in each territory, taking into account the location accuracy and the magnitude homogeneity. We excluded some offshore regions because of their poorer location and magnitude accuracy, as well as their higher completeness magnitude. In addition, we excluded volcanic regions and regions with deep seismicity, since they behave differently from shallow tectonic seismicity. In one case, after a preliminary analysis, we also removed a sub-region (the small orange area in Figure 1, located in northern Italy), where the seismicity characteristics in terms of event frequency differed from those of the rest of the analyzed territory (Brondi et al., 2025). In the corresponding paper, we proposed some hypotheses regarding the physical meaning of this behavior. From a statistical perspective, the clusters in this area belong to a region-specific population distinct from the other clusters, so including them in a joint analysis would introduce bias. Particular care was taken in defining magnitude homogeneity. For example, we used the Southern California Earthquake Catalogue (Hutton et al., 2010), which lists local magnitudes for all earthquakes. However, we did not use the Northern

California Earthquake Catalogue (NCEDC, 2014), despite its similar quality, because it lists different types of magnitude for different earthquakes. For Northern California and the limited data available in western Nevada along the California border, we used the ANSS California Comprehensive Earthquake Catalog (ComCat) when local magnitude data were available as its magnitude assessment aligns well with the Southern California Earthquake Catalogue. For the same reason, we used the revised Lolli and Gasperini (2006) catalogue prior to the start of the ISIDE catalogue in 2005, as it was explicitly proposed to provide compatible magnitude assessment. Catalogues adopted in Italy and NE Italy–W Slovenia after 2020 have been used for applying our methodologies to clusters different from those used for the calibration of the method; these are the real-time versions of the catalogues used for previous years. They have been used for near-real-time application of the algorithm..

Table 1 lists the catalogues used for each region.

Region	Time interval	Reference
Italy	1980-2004	Lolli and Gasperini (2006)
	2005-2020	ISIDe Working Group (2007)
	2021-2025	https://terremoti.ingv.it/
NE Italy – W Slovenia	1977-2020	Snidarcig et al., (2020)
	2021-2025	https://terremoti.ogs.it/
California	1980-2023	SCSN earthquake catalog (Hutton et al., 2010)
	1980-2020	ANSS California, Comprehensive Earthquake Catalog (ComCat)
Greece	1995-2023	AUTH earthquake catalogue
Japan	1973-2024	Japan Meteorological Agency seismic catalog (2024)

Table 1: Adopted catalogues in different regions and time period for which they are used

The following sections summarise the tectonic framework across analyzed regions, providing context for interpreting how local structures may affect the occurrence of largest aftershocks within seismic

sequences and how these regional tectonic differences may influence the performance of features used for forecasting strong subsequent earthquakes.

2.1 Italy

One of the regions where NESTORE has been more widely used is Italy (Gentili and Di Giovambattista, 2017; Brondi et al., 2025) - orange in Fig. 1.

Italian seismicity results from the interaction between the African and Eurasian plates and can be divided into five main zones (Gentili and Di Giovambattista, 2017; Brondi et al., 2025):

- **Alps and Dinarides**. This sector was formed by the collision between the Eurasian plate and the Adriatic microplate, which led to crustal compression and uplift. Seismicity is shallow and clustered in the eastern sectors (Friuli, Eastern Alps) and the western regions (Piedmont, Ligurian Alps), while the central Alps are quieter. Historical events include the 1511 Idrija (Mw ~6.8) and 1976 Friuli (Mw 6.4) earthquakes, as well as modern Mw 4–5 earthquakes along thrusts and strike-slip faults. GPS data indicate ongoing deformation consistent with these seismogenic structures (Devoti et al., 2008).
- **Apennine Range.** It is characterised by ongoing extension due to slab retreat, with frequent earthquakes occurring along NW–SE normal faults (http://emidius.mi.ingv.it/CPTI/, Malinverno and Ryan, 1986; Doglioni, 1991, 1995). Major historical and recent events include the 1688, 1805, 1962, 1980 Irpinia, 1984 Abruzzo-Lazio (Milano and Di Giovambattista, 2011), 1990 Potenza (Azzara et al., 1993), 1997 Umbria-Marche (Miller at al., 2004), and 2016 (Amatrice) earthquakes (Calderoni et al., 2017). Seismicity clusters along the active fault network with increasing deformation rates southward.
- **Calabrian Arc and Southern Tyrrhenian Sea**. This is an active subduction margin where the Ionian plate subducts beneath the Calabrian Arc, generating shallow and deep earthquakes (Chiarabba et al., 2008; Doglioni et al., 2007). Notable events include the 1783 Calabria, 1905, and 1908 Messina-Reggio Calabria (Mw ~7.1) earthquakes. Deep-focus quakes reach ~500 km beneath Calabria and the Aeolian Islands, with seismicity reflecting slab rollback and crustal stretching (Polonia et al., 2016). Studies also suggest the presence of a slab tear at the southern edge of the subducting Ionian lithosphere (Polonia et al., 2016), and this tear had been imaged by Godano et al. (2025) using b-more-positive method (Lippiello and Petrillo, 2024) tomography.
- **Southern Tyrrhenian Basin**. A back-arc basin formed by slab retreat, with crustal thinning, extension, and volcanic activity (Aeolian Islands). Seismicity spans from shallow extensional and

volcanic earthquakes to deep events marking the subducting Ionian plate, highlighting the interplay of extension, magmatism, and subduction (Chiarabba et al., 2008).

- **Northern Sicily**. Located at the junction of compressional and strike-slip tectonics between the Sicilian thrust belt and Calabrian Arc. Moderate to strong earthquakes occur inland and offshore, with the 1908 Messina earthquake as a key destructive event. Seismicity is focused along the offshore North Sicily Fault System and inland thrust faults, with seismic risk driven by compression, strike-slip motion, and proximity to subduction (Totaro et al., 2016).

Overall, these diverse tectonic settings - collision zones, extensional belts, active subduction - make Italy a highly seismically active region in the Mediterranean area, with a long history of destructive earthquakes and significant ongoing hazard.

2.2 NE-Italy and Western Slovenia

In addition to the national level, NESTORE was also applied to a region at the edge between Italy and Slovenia (red region in Fig. 1 - Gentili and Di Giovambattista 2020; Brondi et al. 2025) using the regional OGS catalogue (Snidarcig et al., 2020). This area is characterized by reduced spatio-temporal extent of the clusters and a lower productivity in terms of cumulative moment and number of earthquakes (for a given mainshock magnitude) with respect to the Italian seismicity (Brondi et al., 2025). The predominant deformation regime varies from compressional in the western sector to strike-slip in the eastern sector. Several tectonic phases have reactivated old fault structures, leading to a fragmentation of the crust into different tectonic blocks that define the current seismotectonic zonation (Bressan et al., 2003). Seismic activity is mostly concentrated in two main fault systems: the Alpine system with an approximate E-W orientation and the Dinaric system with a NW-SE orientation, respectively in the northern and eastern parts of the region. The earthquakes are shallow and typically occur at a depth of 6-12 km in the western area (Bressan et al., 2012; Bressan et al., 2018) and 2-7 km in the eastern area (Bressan et al., 2009; Gentili and Gentile, 2015; Gosar, 2019). Focal mechanism solutions indicate that thrust faulting prevails in the western part, while strike-slip faulting mechanisms are more common in the eastern part, with occasional normal faulting (Bressan et al., 2016 and references therein). The area experienced several strong earthquakes in the past (11 clusters of seismicity with earthquakes of intensity IX-X from 1117 to 1976 - see e.g. Gentili and Franceschina, 2011) causing death and destruction. After the ML=6.4 earthquake in 1976, lower magnitudes followed, with 10 strongest events with latitudes between 45-46.5

and longitudes between 11.5-14.5 (a rectangle of approximately 230 in longitude and 170 km in latitude) in the magnitude range [4.5-5.6] in the almost 50 years from 1977 to 2025 (Gentili and Di Giovambattista, 2020; Brondi et al., 2025).

2.3 California

The works on seismicity in California (Gentili and Di Giovambattista, 2022; Gentili et al., 2023; Gentili et al., 2023b) represented a significant development of NESTORE. These papers introduced several improvements to the algorithm and code, resulting in NESTOREv1.0, now publicly available on GitHub (Gentili et al., 2023).

California is among the most seismically active regions in the world, located along the complex transform boundary between the Pacific and North American plates (Hauksson & Shearer, 2005). The seismicity of the region is dominated by the right-lateral San Andreas Fault system, the Eastern California Shear Zone, and subsidiary faults such as the San Jacinto and the Hayward, creating distinct seismotectonic domains with different stress regimes and seismic productivity (Trugman & Ben-Zion, 2023).

Southern California, in particular, exhibits high seismicity rates due to the interaction of these major fault systems with a network of secondary faults, resulting in frequent moderate-to-large earthquakes and diverse focal mechanisms (Hauksson & Shearer, 2023). This complexity drives the cluster behavior and aftershock sequences observed across the region and has implications for seismic hazard assessment and operational forecasting (Trugman & Ben-Zion, 2023).

2.4 Greece

The newly developed NESTOREv1.0 algorithm was also applied to the seismicity of Greece (black region in Fig. 1 - Anyfadi, 2023; Anyfadi et al., 2023). Greece lies at the boundary between the Eurasian and African tectonic plates, where the complex and sometimes powerful seismicity is driven by various geological structures, such as: the Hellenic subduction zone, stretching from the Ionian Islands to Crete (Le Pichon et al., 1995), while the North Anatolian Fault, a major strike-slip fault extending from Turkey into the Aegean region that transfers deformation westward. The Hellenic Subduction Zone is one of the dominant geodynamic features in the eastern Mediterranean region. The Mediterranean lithosphere subducts beneath the back-arc area of the South Aegean Sea, the tectonics of which are mainly driven by a regional field of extension (McKenzie, 1978). The complex geologic setting of the Aegean is dominated by two tectonic processes. The first is the northward movement and subduction of the African plate

beneath the Aegean at a rate of 0.9 cm/year (Reilinger et al., 2010; McClusky et al., 2000), resulting in the formation of the Hellenic subduction zone, while the second is the southward migration of the Aegean plate due to the African slab rollback. The subduction of the African plate formed the Wadati-Benioff zone in the southern Aegean which extends down to about 170 km (Papazachos et al., 2000). The southern Aegean itself is a region where high seismicity is occurring along the forearc. On the other hand, the back-arc region is characterized by moderate seismicity except from its eastern part (Dimitriadis et al., 2010). In the front of the Hellenic Arc, Crete, endures intense seismic activity due to active subduction and regional extension. Fault systems on Crete align in multiple directions, with the most recent and active normal faults trending WNW–ESE and NNE–SSW. The interplay of arc-parallel and arc-perpendicular extension contributes to significant vertical and horizontal displacements (Delibasis et al., 1999; Vallianatos et al., 2022). Furthermore, in the Western part of Greece the Cephalonia Transform Fault, marks the transition between the subduction zone of the Hellenic Arc and the zone of western Greece. In Central Greece the Corinth Rift is rapidly extending and highly active break-up zone (Ambraseys and Jackson, 1997; Sakellariou et al., 2007).

In addition, the Peloponnese region experiences extensional tectonics with major active normal faults trending NE–SW and WNW–ESE, influenced by the subduction zone to the southwest and the Corinthian Gulf to the north (Koukouvelas et al., 2010). Thessaly in the main land of Greece, shaped during the Neogene–Quaternary period, is characterized by a network of normal faults, grabens, and horsts trending NW–SE and E–W. These faults result from ongoing N–S and NE–SW extensional forces and demonstrate a mix of active normal, reverse, and thrust faulting, especially along the edges of major mountain ranges like the Pindos (Caputo and Pavlides, 1993). Southern Thessaly is seismically active with several large earthquakes over the past century, while northern Thessaly, despite similar geological conditions, shows significantly less seismicity (Caputo, 1995; Vallianatos et al., 2021).

In northern Greece, the Central Macedonia region lies within the Inner Hellenic orogeny and exhibits complex tectonics. The extension of the N-S to NE-SW high-angle (50–80° dips) (Gkarlaouni et al., 2015) normal faults and rift basins formed since the Miocene and are consistent with the Aegean back-arc tectonics. The Mygdonian graben, aligned NW–SE, is especially active, reflecting a broader N–S extensional regime tied to back-arc spreading behind the Hellenic subduction zone. In the Halkidiki peninsula, faults trend NW–SE, E–W, and N–S, with notable systems like the Stratoni-Varvara and Gomatius faults (Alatza, 2013). Overall, the seismic activity in mainland Greece and its islands is shaped by a combination of extensional and compressional forces, leading to a variety of seismotectonic regimes and making it one of the most interesting areas for the implementation of NESTORE algorithm.

2.5 Japan

The last published application in chronological order of NESTORE is Japan seismicity (blue region in Fig.1 - Gentili et al., 2025). Japan's seismicity is mainly driven by the convergence of multiple tectonic plates. The Pacific Plate subducts beneath the Eurasian Plate along the Japan Trench, producing powerful megathrust earthquakes. In the southwest, the Philippine Sea Plate also subducts beneath the Eurasian Plate, generating significant interplate seismicity along the Nankai Trough. Subduction rates are high—approximately 9–11 cm/year for the Pacific Plate and 6–11 cm/year for the Philippine Sea Plate (DeMets et al., 2010; Argus et al., 2011; Wu et al., 2016). In the north, interactions between the Eurasian and North American Plates contribute to complex seismic patterns. Japan's earthquake distribution is highly heterogeneous and reflects the complex interplay between these tectonic systems. The eastern offshore region, encompassing the Japan Trench, is characterized by frequent intermediate to large subduction earthquakes. The southwestern margin, particularly along the Nankai Trough, has a well-documented history of great earthquakes occurring in segmented patterns (e.g., the 1944 Tonankai and 1946 Nankai events – Kanamori, 1972). Inland Japan is also seismically active due to crustal deformation resulting from the ongoing plate convergence. Numerous active faults, such as the Itoigawa – Shizuoka Tectonic Line and the Japan Median Tectonic Line, accommodate inter-plate stress and can generate damaging shallow earthquakes, but these are just examples of regional-scale structures. Nonetheless, the seismicity is not confined only to the plate boundaries: very strong earthquakes occur also in central and western Honshu, Kyushu, and the Niigata and Nagano with reverse or strike-slip faulting. Volcanic activity is another important source of seismicity in Japan, with hundreds of volcanoes distributed all along the islands of the archipelago with most of them still active. These volcanoes are associated with magma-induced seismic swarms and shallow VT earthquakes. In March 2011, the Tōhoku earthquake sequence occurred, starting with a Mw 7.3 foreshock on March 9, followed by the devastating Mw 9.1 mainshock on March 11. This event triggered a massive tsunami, resulting in significant human and environmental losses, including the Fukushima Dai-ichi nuclear disaster. The mainshock ruptured a ~400 km long segment of the subduction interface with an estimated slip of ~50 meters (Lay, 2018), highlighting the destructive potential of subduction zone earthquakes. It was one of the largest earthquakes ever recorded. While events of this magnitude are rare, over 80 earthquakes with $M \geq 7$ were recorded between 1973 and 2023 in Japan and surrounding areas belonging to the Asia-Pacific region. To define the study area, we considered factors such as completeness magnitude, seismic network coverage, and the distribution of volcanic seismicity. Mount Fuji and Miyake Island, for instance, were excluded by our study.

3. Methods

NESTOREv1.0 consists of four main modules: the cluster identification module, the training module, the testing module, and the Near-Real-Time (NRT) classification module. The key advancements during these years of NESTORE development lay in the enhanced cluster identification methodology and the implementation of stringent quality criteria for the training dataset and result validation, aimed at improving the algorithm's generalization capability (Brondi et al., 2025; Gentili et al., 2025). The modularity of the approach allowed us to substitute the cluster identification module if it was not effective for the current dataset as in the Japan seismicity case (Gentili et al., 2025).

In all versions of NESTORE, the analysis starts when an earthquake exceeding a certain magnitude threshold occurs, provided it is not part of any previously identified cluster. This event is termed the "operative mainshock." (or o-mainshock). This concept is used because NESTORE aims to produce near-real-time forecasts during the early evolution of a seismic cluster, assessing the probability of a strong event occurrence after a moderate to intense o-mainshock. It's important to note that the operative mainshock may not be the actual mainshock of the cluster, as the true mainshock might not have occurred yet at the time of the forecast.

3.1 Cluster identification and selection

The easiest way to select clusters corresponds to the so-called window based methods, which consider as belonging to the same cluster all the events within a given radius and time window from the stronger one(s). NESTOREv1.0 code (Gentili et al., 2023) allows to select clusters applying user-defined windows based on the magnitude of the stronger event(s). This method (see section 3.1.1) supplied good results for most clusters in Italy, Western Slovenia, California and Greece (Gentili and Di Giovambattista, 2017, 2020, 2022; Anyfadi et al., 2023; Brondi et al., 2025; Spassiani et al., 2025), while the application to Japan required a further, more complex approach. In fact, identifying earthquake clusters in Japan poses significant challenges due to the region's high seismicity rate and the spatial-temporal overlap of nearby sequences (Gentili et al., 2025).

3.1.1 Window based method

In the window-based method, any event with a magnitude Mm greater than a fixed threshold Mth is considered as a potential main earthquake. The corresponding aftershocks of the cluster are detected in

space and time by using a circular region centered on the epicenter of the main earthquake and a temporal window, both the radius of the circle and the time duration depending on Mm. If a potential mainshock is in the cluster spatio-temporal window of a previous one, the two clusters are merged, and only one of the two is considered the mainshock. The radius and the duration of the cluster are defined based on some equations, generally referred to as: <Proposer's name> (<year>) law. We selected different laws for different analyzed areas, comparing different laws existing in literature with real data (further details in the corresponding papers). In detail, we used the following laws for each area:

- Uhrhammer (1986) and Lolli and Gasperini (2003) laws for the spatial and temporal selection of aftershocks, respectively, in Italy.
- Gentili and Bressan (2008) laws for both space and time for NE Italy - Western Slovenia; in order to take into account the inaccuracies in localization in the first years of the catalogue, 2 km have been added to the radius for the spatial selection.
- Kagan (2002) law for space and Gardner and Knopoff (1974) law for time in California.
- Uhrhammer (1986) for both space and time windows in Greece.

3.1.2 GRETAS: a method based on stochastic declustering

Traditional window-based methods proved inadequate because clusters from different sources often occur close in both time and space. This can lead to incorrect associations and contamination of clusters, negatively affecting the performance of classification algorithms such as NESTORE.

To overcome these limitations, we implemented a hybrid cluster identification method that integrates probabilistic and deterministic elements. The core of the method is based on the stochastic declustering algorithm developed by Zhuang et al. (2002), which models seismicity using the Epidemic-Type Aftershock Sequence (ETAS) model (Ogata, 1988). In this framework, each event may be either a background (independent) earthquake or may be triggered by a previous one, with associated probabilities estimated through maximum likelihood.

The ETAS model defines the conditional intensity function as the sum of a background term and a triggering term that accounts for the contributions of all preceding events. This includes temporal decay (Omori-Utsu law), spatial decay, and productivity scaling with magnitude. The model assumes magnitude independence between triggering and triggered events (Petrillo and Zhuang 2022, 2023).

ETAS model parameters are estimated using the original iterative algorithm by Zhuang et al. (2002) and Ogata and Zhuang (2006), ensuring reproducibility with prior studies.

Each event in the catalog is assigned a probability of being background or being triggered by a specific preceding event. The stochastic declustering proceeds by generating a random number and assigning each event to the background or to a parent event probabilistically. Because of its stochastic nature, the clustering output varies across realizations.

The new algorithm proposed in Gentili et al. (2025), here referred to as GRETAS (GRaph-based approach to ETAS), treats the output of ETAS from the graph approach point of view. Different runs of the stochastic declustering algorithm supply a set of clusters that can be represented by oriented graphs (trees) that are different from one run to the other depending on the values of the random numbers generated by the algorithm. The nodes of the trees are the earthquakes, while the weight of the arcs between events n (parent) and j (descendent) is related to the probability for the event j of being background and to the sum of probabilities that j is descendent of events until n. The arc is generated only if its weight is larger than the random variable. The events that are strongly connected within a cluster, i.e. the ones that are close in space and time to several previous events, tend to remain grouped together across all runs of the Stochastic Declustering method. This persistence is due to the j-th event typically stays in the cluster because it is linked to multiple other events, not just one. For this reason, we chose to define cluster belonging based only on events that show strong and consistent connections to others. In order to do this, we run the stochastic declustering several times (in Gentili et al., 2025 we chose 10 times). For each mainshock (defined as the largest event in the cluster), we identified the corresponding cluster members by intersecting the outcomes of the different runs. Only those events that were consistently associated with the same mainshock across multiple runs were retained. This ensures that the final clusters include only the most stably connected events, avoiding the inclusion of loosely connected or ambiguous events that may belong to overlapping sequences.

To avoid excessive spatial spreading of clusters, the last part of GRETAS algorithm applies a final spatial filter selecting only earthquakes within a given distance from the mainshock. In Gentili et al (2025) we selected for Japan the empirical law of Uhrhammer (1986). However, this constraint had a marginal effect on the results, removing less than 1% of events.

This robust identification process was applied uniformly to both the training and testing datasets, ensuring consistency in cluster definition throughout the study.

3.2 NESTORE training, testing and Near Real Time modules

3.2.1 Training

The clusters identified in the cluster identification module are the inputs for the training module. Nine features related to the seismic productivity and spatio-temporal evolution in terms of radiated energy, magnitude, number of events and their spatial distribution are computed at different time intervals starting soon after the operative mainshock (for further details on the time start see Gentili et al., 2023) and a threshold is estimated for each of these features to distinguish type A clusters from type B clusters. Typically, most type A clusters have feature values above this threshold, whereas, in contrast, most type B clusters have values below this threshold. The training routine consists of four steps: (1) feature extraction, (2) decision tree training, (3) selection of the time intervals characterized by good performance for each feature (good interval), and (4) inheritance and validation. Since several improvements have been done during time, we describe here the training for versions of the algorithm starting with Brondi et al. (2025).

Feature extraction

The features, detailed in Section 3.3, are extracted from events with magnitude greater or equal to Mm-2 in 10 time intervals Ti, starting s_1=1 minute after the occurrence of the o-mainshock and ending at steps of 6 hours on the first day and 24 hours on the first week.

Decision tree training

For each feature, a one-node decision tree is trained in each time interval so that, if the tree converges, it finds a threshold above which the majority of the feature values of the type A clusters lie. If no threshold value can be found, the feature is discarded for this time interval.

Selection of good interval

The reliability of the determined threshold values is tested with a k-fold cross-validation method with k=1, the so-called “Leave One Out” (LOO) method, which is particularly suitable for small training data sets (i.e. the order is of the dozens of cases). The performance of the decision trees is evaluated based on four statistical properties: Accuracy, Precision, Recall (ranging between 0 and 1) and Informedness (ranging from -1 to 1). These evaluators are used for binary classifiers performance evaluation. The two classes are defined as “positive” and “negative”. In our case we considered the type A class as positive class and the B as negative. The Accuracy is defined as the percentage of correct classifications. The Precision is defined as the percentage of samples classified as positive that are actually positive. The Recall is defined as the percentage of correct classification of positives; vice-versa, the Inverse Recall,

is the percentage of correct classification of negatives. All these percentages are normalized to 1. The Informedness is the sum of the Recall and the Inverse Recall -1 and is a measure on how informed the classifier is about the classes.

A feature is used by NESTORE in a certain interval, which is defined as “good interval", if the evaluators fulfill certain criteria:

- Accuracy, Precision and Recall are strictly above 0.5;
- Accuracy is equal to or greater than that of a tree classifying each cluster in the more populated class;
- Informedness is strictly greater than 0;

The Good interval ends at a time less than or equal to s2 when the Informedness is maximal. The feature value and the threshold value for s2 are “inherited” into the subsequent time intervals.

Inheritance and validation

The constancy of the calculated and inherited feature values and thresholds is reinforced by reapplying the LOO method by calculating the percentage of correct classification of type A clusters (Recall or True Positive Rate) and the percentage of incorrect classification of type B clusters (False Positive Rate) for each Ti. The feature thresholds of the Ti intervals in which the false alarm rate is greater than the Recall are discarded. For the selected features and time intervals, the probability that the cluster is of type A when the feature value is above or below the threshold is estimated from the training set as the percentage of A clusters with this feature above or below the threshold. Since the method is applied to real data, the probability may be less than 1 above the threshold and greater than 0 below the threshold due to noise or imperfect performance of the feature in discriminating the cluster typology.

3.2.2 Testing

The testing module uses the values determined in the training module to forecast the class type of the clusters of an independent test set. For each cluster of the test set, the features selected in the training phase are calculated in the 10 time intervals Ti from the operative mainshocks of this new data set and, depending on whether they are above or below the training threshold, the probability that the cluster belongs to type A is estimated for each feature and each time interval Ti.

Let $p_{n,i} = P(A|F_{n,i})$ be the probability that the cluster is of type A for the n^{th} feature Fn in the i-th time interval. In more recent versions of NESTORE (first use in Gentili and Di Giovambattista, 2020) these

probabilities are combined using a Bayesian approach to calculate the overall probability P that the cluster is for type A for each time interval Ti

$$P_i(A \mid F_{1,i} \dots F_{N,i}) = \frac{[N(B)_i]^{N-1} \prod_{n=1}^{N} p_{n,i}}{[N(B)_i]^{N-1} \prod_{n=1}^{N} p_{n,i} + [N(A)_i]^{N-1} \prod_{n=1}^{N} (1-p_{n,i})} \quad (1)$$

where N(A)i and N(B)i are the number of clusters A and B at time Ti in the training dataset. It is important to know how many samples there are for each class to account for the possible imbalance between classes. The equation (1) was obtained from equations of Bailer-Jones and Smith (2011) for combining probabilities from different independent features $D_1 \dots D_n$:

$$P(C|D_1 \dots D_N) = a \frac{\prod_{n=1}^{N} P(C|D_n)}{P(C)^{\{N-1\}}} \quad (2)$$

Where $P(C)$ is the probability to have class C, $P(C|D_n)$ is the posterior probability that class is C given D_n, and a is a normalization factor such that $\sum_k P(C_k|D_1, \dots D_N) = 1$.

In our case, we assumed that the probability of the classes A and B corresponds to the fraction of instances of that class in the training set. See Gentili and Di Giovambattista (2020) for further details. The output of the testing module of NESTOREv1.0 is the estimation of the cluster type, expressed as a probability P(A).

In order to estimate the performance of the method, the forecasting about A-type or B-type clusters is provided by comparing the resulting probability P(A) with the threshold equal to 0.5: if P(A)≥0.5 the cluster is classified as A-type, otherwise as B-type. The comparison of the output classification with the actual class of the cluster provides an estimate of the performance of the algorithm, which is described by the Receiving Operating Characteristics (ROC) and the Precision-Recall diagrams. Examples of the result diagrams can be found in Section 4.1.

Note that due to the small dataset available, validation is performed during the training using the LOO method and for the individual features. The merging of the features' performance is only carried out in the testing phase, and there is no validation set to determine the best interval for each analyzed region. For simplicity, we here only show the best results in the dedicated section, but all data can be found in the corresponding articles.

3.2.3 Near Real Time Application

The Near Real Time (NRT) module is the latest development of NESTOREv1.0, which aims to forecast the class type of an ongoing seismic cluster. The first description of this module is in Gentili et al. (2023).

According to the general procedure of NESTORE, the cluster is defined with a window-based, magnitude-dependent method from the mainshock, which also determines the time and area for the forecasting. The features are calculated for increasing time periods Ti until the one for which the testing procedure estimated the classification performances are the best , and compared with the corresponding values and thresholds obtained in the training for the study area. The NRT output consists of a map of the cluster in each time interval and the class forecast, given in the form of an AFtershock-based Traffic Light System (AFTLS - Gentili et al., 2023). The AFTLS colors are related to the probability of occurrence of a strong aftershock: red for high probability (type A), green for low probability (type B), yellow for uncertain assessment.

Before applying the NRT module, the training is redone with all the available data (training set and test set) in order to obtain more stable thresholds; like in the case of the previous training, the validation is performed by the LOO method, without using a dedicated validation set. In Brondi et al. (2025) and Gentili et al. (2025) the thresholds obtained with the larger dataset are compared with the previous ones detailing which are stable and which are improved. Since the NRT module needs an estimate of which are the more reliable time intervals for the forecasting, but no proper validation set is available, this information is taken by the output of the testing phase (see conclusion and discussion for further details).

3.3 NESTORE features

The features used in NESTORE (see Gentili et al., 2025) are related to the spatiotemporal distribution of the aftershocks, the source area, the magnitude trends and the radiated energy. They are calculated for events with magnitude in the range [Mm-2, Mm], chosen in order to account for the possible incompleteness of the catalog.

1. S: normalized event source area

   $$S(i) = \sum_i 10^{(m_i - M_m)} \quad (3)$$

   where m_i is the i^{th} event magnitude.

2. Z: linear concentration of events

   $$Z(i) = \frac{mean(10^{0.69 m_i - 3.22})}{mean(r_{ij})} \quad (4)$$

   with r_{ij} being the distance between the i^{th} and j^{th} events

3. Q: normal radiated energy

   $$Q(i) = \frac{\sum_i E_i}{E_m} \quad (5)$$

being E_m the mainshock energy, and E_i the energy of the ith event

4. SLCum: Cumulative deviation of S from the long-term trend on increasing length windows
$$SLCum(i) = \sum_i abs[S(t_i) - S(t_{i-1})]\frac{i \cdot dt}{(i-1) \cdot dt} \quad (6)$$
5. SLCum2: Cumulative deviation of S from the long-term trend on sliding windows
$$\mathrm{SLCum2(i)} = \sum_{\mathrm{i}} \mathrm{abs}[\mathrm{S}([s_1 + (\mathrm{i}-1) \cdot \mathrm{dt},\ s_1 + \mathrm{i} \cdot \mathrm{dt}]) - \mathrm{S}([s_1 + (\mathrm{i}-1) \cdot \mathrm{dt}, s_1 + (\mathrm{i}-1) \cdot \mathrm{dt} + \mathrm{d}\tau])\frac{\mathrm{dt}}{\mathrm{d}\tau}] \quad (7)$$
6. QLCum: Cumulative deviation of Q from a long-term trend on increasing length windows
$$QLCum(i) = \sum_i abs[Q(t_i) - Q(t_{i-1})]\frac{i \cdot dt}{(i-1) \cdot dt} \quad (8)$$
7. QLCum2: Cumulative deviation of Q from the long-term trend on sliding windows
$$QLCum2(i) = \sum_i abs[Q([s_1 + (i-1) \cdot dt,\ s_1 + i \cdot dt]) - Q([s_1 + (i-1) \cdot dt, s_1 + (i-1) \cdot dt + d\tau])\frac{dt}{d\tau}] \quad (9)$$
8. Vm: Cumulative variation of magnitude from event to event
$$V_m(i) = \sum_i |m_i - m_{i-1}| \quad (10)$$
9. N2: Number of events with magnitude ≥Mm-2
$$N_2(i) = \sum_i H[m_i - (M_m - 2)] \quad (11)$$
where H is the Heaviside step function

In the case of the application of NESTORE to Japan (Gentili et al., 2025), we substituted N2 with:

$$9'.\ N_{2S}(i) = N_2(i) + 110 \cdot S(i) \quad (12)$$

which performed better in that area.

3.4 Data cleaning by outliers removal - REPENESE algorithm

The biggest challenge of NESTORE is the classification of small and often very unbalanced data sets as e.g. in the Japanese seismicity case. For this reason, starting with the paper of Gentili et al. (2025), we developed the REPENESE (RElevant features PErcentage class weighting NEighborhood detection SElection) algorithm. A preliminary assessment of the quality of the training dataset is essential to achieve reliable results, and to establish more appropriate thresholds for discriminating between cluster populations. The detection of outliers must fulfill three important requirements: (1) the selection should

be based solely on relevant features, (2) the imbalance between classes must be taken into account (removing a rare cluster of type A is more critical than removing a frequent cluster of type B), and (3) the standard centroid distance methods such as Z-score (Rousseeuw and Hubert, 2011) should be replaced by a threshold-based approach, since correct classification depends on position relative to a feature threshold rather than proximity to a centroid.

To overcome these challenges, we have developed a custom outlier detection method called REPENESE (Gentili et al., 2025), which involves four steps:

- **RE (RElevant Features):** Features are selected as relevant if a threshold exists and the True Positive Rate > 0.5, the False Positive Rate < 0.5, and Precision > 0.5.
- **PE (PErcentage class weighting)**: The imbalance between the classes is quantified using the probabilities P_A and P_B calculated from the relative frequencies of clusters of type A and B in the training set.
- **NE (NEighborhood detection):** Neighborhoods are defined for each relevant feature based on the sorted feature values. Type A samples consider the nearest N_1 (set to 5) larger values; type B considers the N_1 smallest values.
- **SE (SElection):** A sample of a given class (A or B) is labeled as an outlier if the number of samples of the same class in its neighborhood does not exceed P·Sn, where Sn is the size of the neighborhood and P is the probability P_A or P_B respectively. Only samples that are consistently identified as outliers across all relevant features and thresholds are removed from the training set.

This method increases the robustness of the training set by ensuring a better representation of minority classes and reducing noise, which ultimately improves the generalization capability of the model.

4. Results

This section summarizes the more recent results for Italy, northeastern Italy and western Slovenia, California, Greece and Japan. For California, we refer to the results available on GitHub and Zenodo (Gentili et al., 2023), where a more recent version of the code is available than in the paper by Gentili and Di Giovambattista (2022).

In Sections 4.1. we compare the training and testing performances in different regions. Section 4.2 provides some results on the NESTORE thresholds in different regions, outlining their differences. Section 4.3 yields further statistical information on the evolution of the clusters in space-time and the seismic moment, which can be provided together with the class of the cluster at the time of forecasting.

Finally, the Near Real Time application of NESTORE is presented in Section 4.4. In the Discussion and Conclusions section the outcome of the results is discussed.

4.1 Training and testing

The clustering module identifies seismic clusters from the input catalogs. However, not all clusters are suitable for NESTORE. Clusters are discarded under various conditions: (1) if the mainshock is outside of the definition areas (see Fig. 1); (2) if the strongest aftershock occurs within the first six hours after the mainshock, limiting the availability of statistical data; (3) if the magnitude of the strongest aftershock falls within the range of $Mm-1\pm0.2$, to avoid incorrect class assignments due to inaccuracies in magnitude estimation; (4) if the completeness magnitude is greater than Mm-2.
The cardinality of the refined training set we used for the first 6-hour time interval of each analysed area is shown in Table 2.

Region	Dataset	Period	No. Clusters	No. A Clusters	No. B Clusters
California	Training	1981-2019	50	21	29
	Testing	1981-2023	13	4	9
Greece	Training	1995-2015	46	6	40
	Testing	2016-2022	27	6	21
Italy	Training	1980-2009	24	7	17
	Testing	2010-2020	14	6	8

NEItaly-WSlovenia	Training	1977-2009	13	4	9
	Testing	2010-2021	18	3	14
Japan	Training	1973-2004	50	7	43
	Testing	2005-2023	31	4	27

Table 2: Training set and Test set cardinality for the analysed areas.

The table shows how the ratio between the number of clusters of type A and B changes from region to region and how in Japan and Greece the classes are highly unbalanced, with the cardinality of class B being 6-7 times higher than that of class A. In order to account for the class imbalance and the presence of outliers, we introduced in our work on Japan the algorithm REPENESE (see section 3.4). After its application, the number of type A clusters in the training set decreased from 11 to 7, the type B from 45 to 43 (the final number is the one used for training and shown in the table).

The cluster selection process described above (points 1-4) is applied also on the clusters of the test set, but the REPENESE algorithm is not applied, because the outliers should be taken into account in the performance evaluation. See Table 2 for the cardinality testing datasets of all the analysed regions.

The performance of NESTORE in the different regions varies according to the region characteristics, the quality of the catalogue, the number of available clusters, the balance of the classes A and B, and so on. In the articles on NESTORE, the testing module estimates and visualizes the performances through the ROC and Precision-Recall diagrams, suitable for binary classifications. In Figure 2 we show the results corresponding to the time interval Ti for which we had the best performances of the algorithm in the analyzed regions. The ROC diagram (see Fig. 2a) shows on the ordinate axis the True Positive Rate (the Recall), i.e. the percentage of correctly classified positives that in our case is the percentage of correctly forecasted as A-type clusters (normalized to 1); on the abscissa axis it shows the False Positive Rate, which in our case corresponds to the percentage of B-type clusters incorrectly classified as A-type (normalized to 1). The dashed line corresponds to a random response. All applications are clearly above

the random response and close to the ideal classification, that is the one in which the True Positive Rate is equal to 1 and the False Positive rate is equal to 0.

If the negative class (in our case class B) has a much greater cardinality than the positive one, even if a small percentage of the negative class is misclassified as positive, a large percentage of the events classified as positive can be misclassified.

A crucial parameter to evaluate in the case of a heavily imbalanced class distribution is therefore the Precision, which in our case is the percentage of clusters classified as A-type that are actually A-type. This information is shown in the Precision-Recall diagram (see Fig. 2b). Horizontal dashed lines show the response of a random classifier, i.e. a value of Precision equal to the normalized percentage of Type-A clusters in the dataset for different regions in the test set. Also in this case, the performance in different regions is close to the ideal classification Precision=Recall=1 which corresponds to the upper right corner.

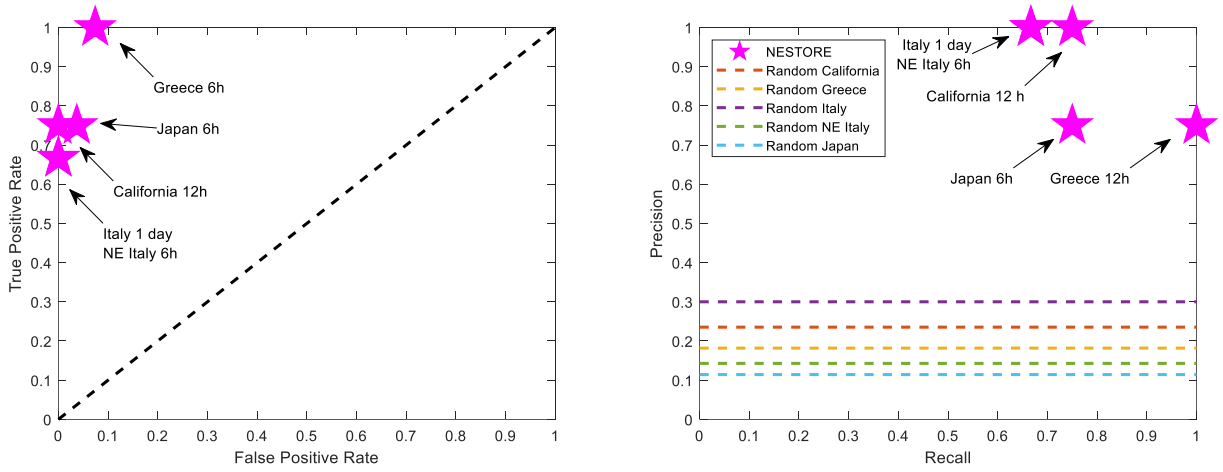

(a) (b)

Fig. 2: Performances of NESTORE in different regions

The large unbalancing of the classes of the test set in Japan and Greece (corresponding to a low value of random classifier precision) slightly affects the Precision in the two regions, which is however greater than the 70%. In the case of NE Italy, no Type-B cluster is misclassified so that the Precision is 1.

As a further analysis, in order to validate our results, we estimated the probability α of obtaining h or more hits (Type A clusters correctly classified) by chance accordingly with Zechar (2010) as:

$$\alpha = \sum_{i=h}^{N} \binom{N}{i} \tau^i (1-\tau)^{N-i} \quad (13)$$

In this case, τ, the fraction of the time-space occupied by alarms is simply the ratio between the clusters classified as A and all and the number of all the clusters; unlike applications in evaluating mainshock forecasting, in which the measure of time-space may be not uniquely defined, in this particular application τ is uniquely defined, avoiding ambiguous results; in this case N is the number of observed type A clusters. A small α corresponds to an alarm with high skill.

Table 3 shows the value of α for the different analyzed regions. Note that for all the cases we analyzed the number of Type A clusters in the training set was unchanged respect to the one of Table 2, even when longer time intervals are considered, so we do not specify here.

Region	Time interval	α
California	12 hours	4.06 %
Greece	6 hours	0.07 %
Italy	24 hours	5.97%
NE Italy- W Slovenia	6 hours	3.41 %
Japan	6 hours	3.36 %

Table 3: Values of α for the different regions

In all cases the probability α of obtaining h or more hits by chance is very low, smaller than the 6%. The highest value is obtained for Italy, where two Type A clusters were wrongly classified. However, a detailed analysis (Gentili et al., 2024) of one of the two clusters which occurred in Molise (Southern Italy) in 2018 showed how its misclassification may be due to an incorrect cluster identification due to effects related fluids diffusion. Considering the proposed cluster definition of Gentili et al. (2024), α reduces to 2.45% and the Recall (True Positive Rate) shown in Fig. 2 passes from 0.67 to 0.83.

4.2 Comparison between features' threshold

In this section we compare the features thresholds we found in different regions (Italy, North East Italy and Western Slovenia, California and Japan) by analysing the results of the papers from 2023 (Gentili et al., 2023; Anyfadi et al., 2023; Brondi et al., 2025; Gentili et al., 2025).

For this purpose, in Fig. 3 we show, when available (Italy, North East Italy and Western Slovenia, Japan), the thresholds obtained from the whole dataset after the outliers removal, being the most stable characterization of the areas. Since for all cases the best performances were obtained with time intervals smaller or equal to 1 day, only these thresholds are compared. Note that the values for Italy and NE Italy-W Slovenia may differ, as the Italian seismicity is dominated by the Apennines' one (Brondi et al., 2025), which is different from the Alpine-Dinaric seismicity in NE Italy. The thresholds inherited from previous intervals are not shown. For details on the thresholds obtained during the original training, please refer to the corresponding papers.

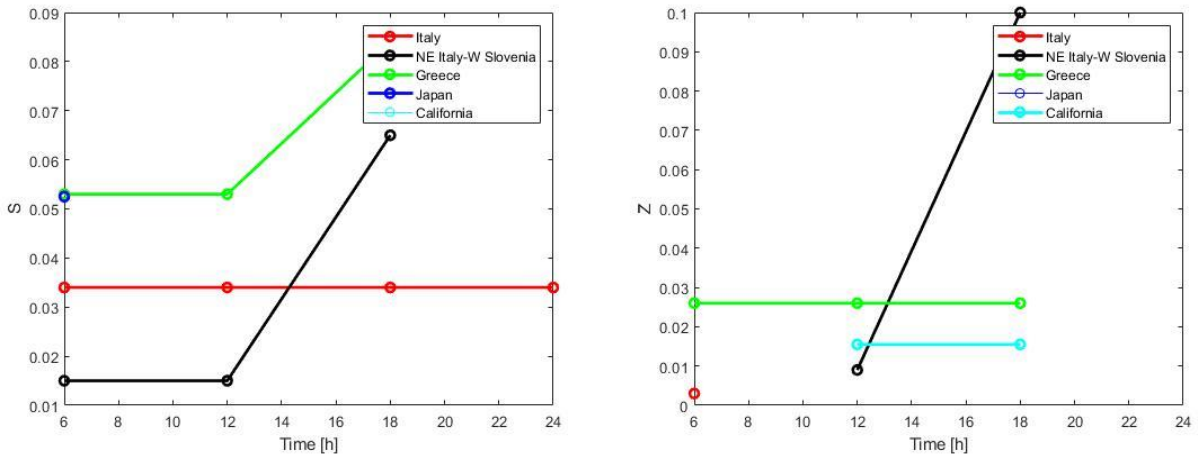

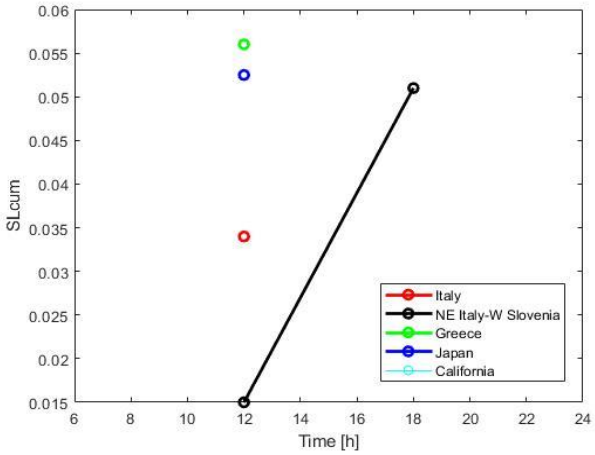
SLcum
Time [h]
Italy
NE Italy-W Slovenia
Greece
Japan
California

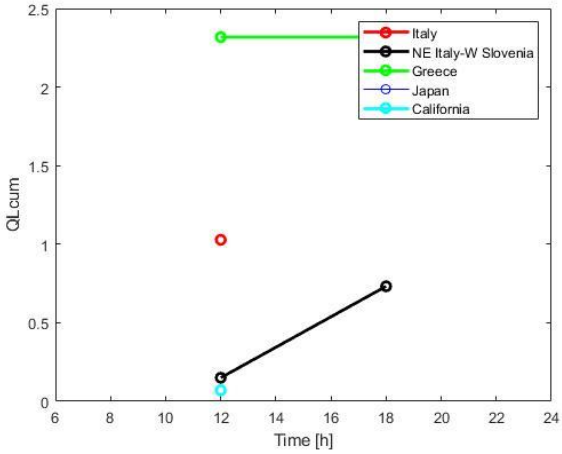
QLcum
Time [h]
Italy
NE Italy-W Slovenia
Greece
Japan
California

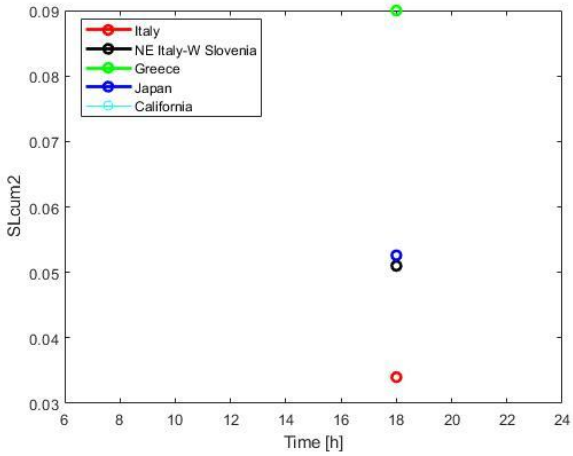
SLcum2
Time [h]
Italy
NE Italy-W Slovenia
Greece
Japan
California

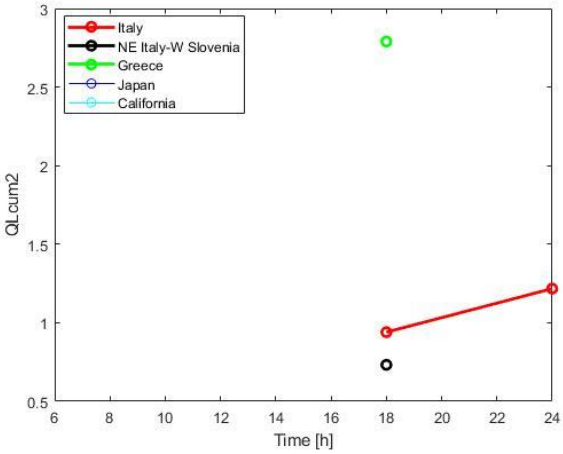
QLcum2
Time [h]
Italy
NE Italy-W Slovenia
Greece
Japan
California

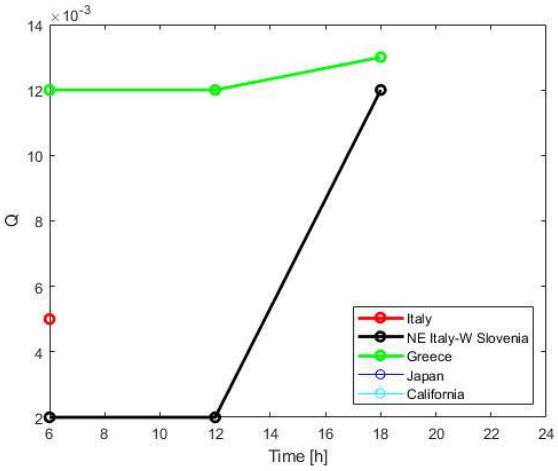
× 10^-3
Q
Time [h]
Italy
NE Italy-W Slovenia
Greece
Japan
California

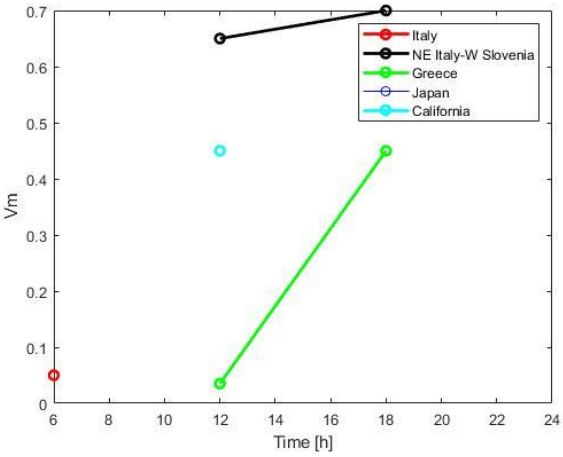
Vm
Time [h]
Italy
NE Italy-W Slovenia
Greece
Japan
California

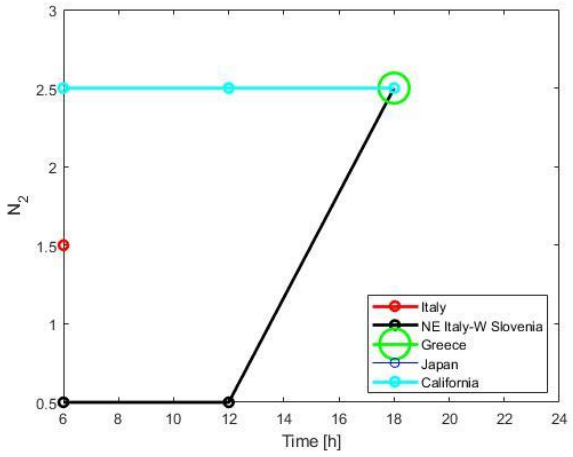

Fig. 3: Thresholds for each feature and time period (when available) for the analyzed regions

As noticeable from Figure 3, all threshold values of the features increase or remain constant with increasing length of the time interval Ti. This is because most features (e.g. the number of events or the radiated energy) are cumulative, so they cannot decrease, and because the larger productivity, especially for B type clusters, occurs in the first hours after the operative mainshock, so some thresholds do not need to increase. When available, the threshold values for the cumulative source area (S), the radiated energy (Q), their time variation (SLCum, SLCum2, QLCum, QLCum2), the number of events (N2) and the earthquake concentration (Z) generally show higher values for Greece and Japan compared to Italy and NE Italy, while California does not show a general trend with respect to the other regions. The feature Vm, which refers to the fluctuation in magnitude from one event to the next, does not show the region-dependent trend of the other features.

Focusing on the partially overlapping areas of Italy and NE Italy-W Slovenia, we see that the threshold values in NE Italy-W Slovenia are lower at short time intervals after the mainshock. The trend is inverted for the time interval ending 18 hours after the mainshock (Brondi et al., 2025). One reason for this inversion could be related to the change in the size of the dataset. Since we only consider clusters of type A that have not yet had the strongest aftershock at the time of analysis, the data set shrinks over time, possibly increasing noise in the data. Another explanation could be a selection effect in the population of type A clusters, if the type A clusters that had the strongest aftershock at a later point in time are also characterised by higher values of the features.

4.3 Further information based on classification

When NESTOREv1.0 was applied to the catalogues of California (Gentili and Di Giovambattista, 2022), Greece (Anyfadi et al., 2023), Italy (Gentili and Di Giovambattista, 2017; Gentili and Di Giovambattista, 2020; Brondi et al., 2025) and Japan (Gentili et al., 2025), type A and B clusters were found to differ in terms of various seismicity characteristics in the first hours or days after the operative mainshock (Gentili et al., 2023; 2025).

Recently, it has been observed that for Italy, NE Italy-W Slovenia (Brondi et al., 2025) and Japan (Gentili et al., 2025), clusters A and B also differ in terms of three parameters measured over the entire duration of the cluster: the effective cluster duration normalised by the cluster duration derived from the window method, the number of aftershocks with a magnitude equal to Mm-2 or more, and the cumulative seismic moment associated with previous aftershocks normalised by the seismic moment of the operative mainshock. In all three areas mentioned, the type A clusters show larger values than the type B clusters in most cases. This corresponds to what was observed with the NESTOREv1.0 features in the first hours after the o-mainshock.

Comparing the distributions of these characteristics for the whole clusters (Brondi et al., 2025; Gentili et al., 2025) in different regions we found the following:

1. Japan and Italy are characterised by a higher number of events with M≥Mm-2 for the A class with respect to NE Italy-W Slovenia (no type A clusters with less than 3 events, while this is the case in northeast Italy-west Slovenia in ⅓ of the cases).
2. Although the minimum value of normalized cumulative seismic moment associated with clusters A is higher in the case of North-Eastern Italy-Western Slovenia, for all 3 areas most clusters A are above 0.2.
3. For the B clusters, the normalized cumulative seismic moment is always confined between 0 and 0.2. and, in detail, always below 0.1 in the case of NE Italy-W Slovenia and Japan. Therefore Italy shows on average a slightly higher B cluster productivity compared to NE Italy-W Slovenia and Japan.
4. Normalized duration of A-type clusters in Italy and NE Italy-W Slovenia are comparable; data of Japan cannot be compared because of the different adopted method of cluster identification. However, in all the cases the normalized duration of type A clusters is generally higher than that of type B ones.

4.4 NESTORE application in Near Real Time

The main goal of the NESTORE algorithm is to provide an alarm when in the first hours/days after a strong earthquake, the features' value of seismicity are consistent with the ones measured for a type A cluster. For this purpose, we proposed a Near Real Time (NRT) module. In the following, we show the performance of the NRT module for the time-intervals corresponding to the best performances in the testing phase. The application of this module to the various regions analysed by NESTORE is at different stages of development. The NRT module is functional for Greece and California, but is not currently being used. In Japan, automatic cluster identification for NRT is still under development, as the window-based methods are not suitable for the seismicity of this area. In Italy and NE Italy-W Slovenia, the NRT module is operational and routinely employed.

4.4.1 Italy

Figure 4 shows the performances of the NRT method in Italy from 2021 to 2024. The analyzed clusters should meet the following requirements:

1. The location must be within the analysis area (see Figure 1);
2. The mainshock magnitude must be greater or equal to 4 (as the completeness magnitude was set to 2 for the whole Italian territory after 2020);
3. No strong aftershock should be recorded in the first six hours after the operative mainshock.

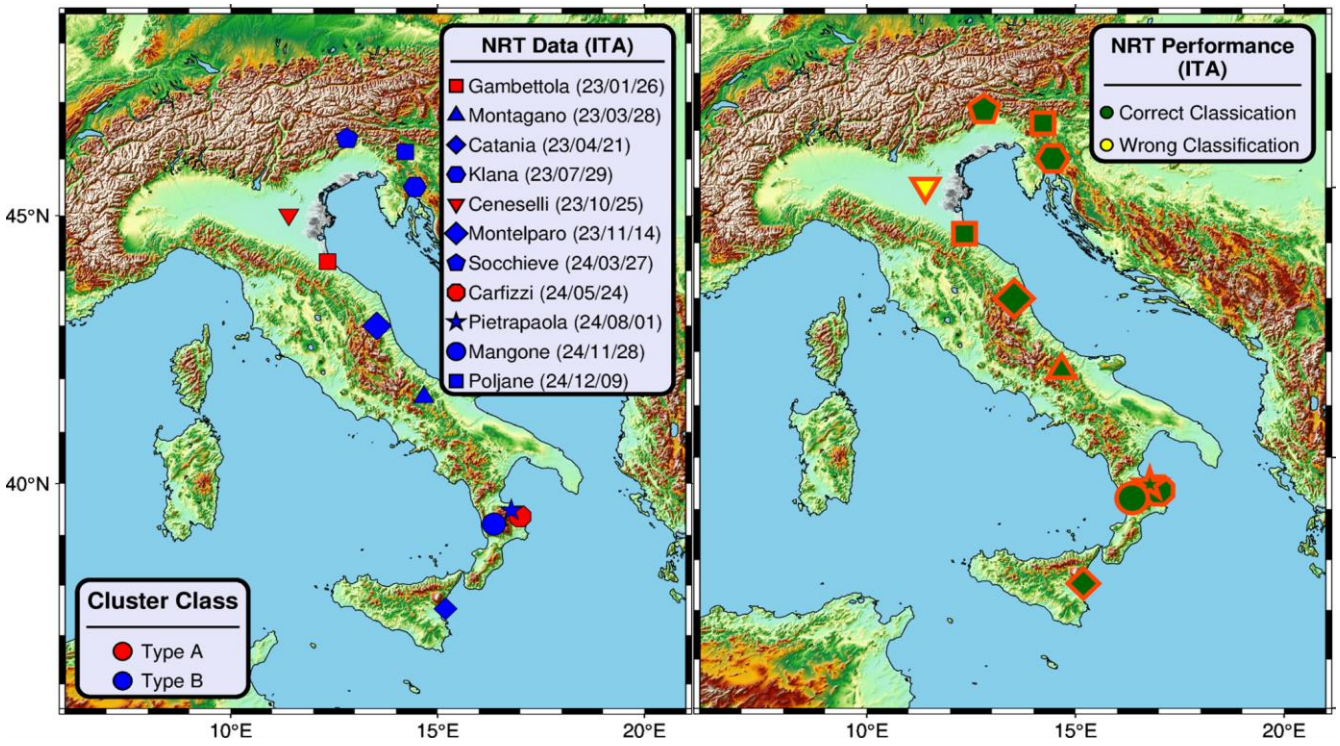

Fig. 4: Near Real Time module performances on INGV catalogue

The code is manually launched when the previous conditions are satisfied. Even though the dataset is not very large due to the short duration of the NRT module evaluation (11 available clusters), the performances of the method are in good agreement with those obtained in the testing phase, with all type B clusters correctly forecasted (False Positive Rate =0), two thirds of type A clusters correctly forecasted (True Positive Rate=Recall=0.66) and all clusters classified as A actually being of type A (Precision=1).

4.4.2 NE Italy and Western Slovenia

Figure 5 shows the performance in NE Italy and Western Slovenia using the OGS catalogue (Snidarcig et al., 2021; Brondi et al. 2024b, 2025b; Real Time Seismology of NE Italy, https://terremoti.ogs.it/). The limited size of the area leads to a dataset that is smaller than the one of the entire Italian territory. Originally, the NRT module was started manually after the occurrence of an earthquake with a magnitude ML≥3.7 that was not already part of an analysed cluster. Since March 2024, the analysis has been carried out automatically (see next section).

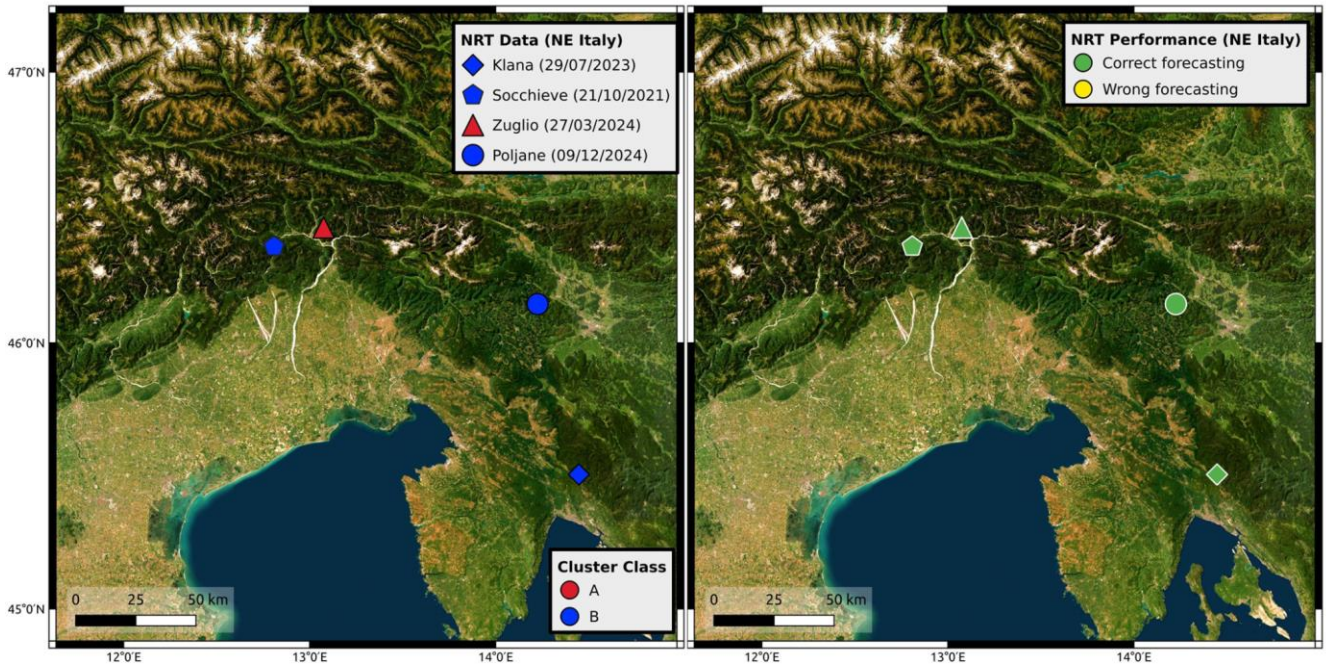

Fig. 5: Near Real Time module performances on OGS catalogue

All clusters analysed through the NRT were correctly forecasted. As with training and testing, the eastern part of the area is characterized by type B clusters. The NRT algorithm is applied automatically from 2024 to the monitoring system managed by the department CRS (Seismological Research Centre) of OGS. For further details see the appendix.

4.4.3 Greece

In Greece the NRT module has not been applied in a systematic way, but it was applied in the thesis work by Anyfadi (2023). A total of four clusters were analysed (see Fig. 6), including data from 1995 to 2022, the 75% of which were correctly classified.

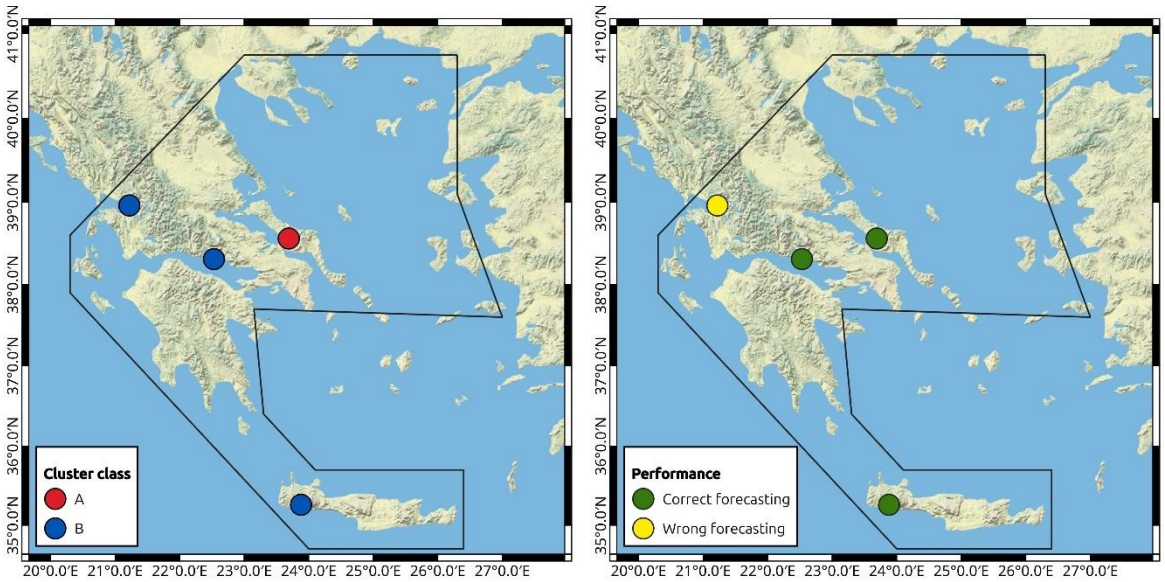

Fig. 6: Near Real Time module performances on AUTH catalogue

Among the three type B clusters, one was misclassified as type A. The Mm = 4.9 type A cluster, located in the Evia area, was correctly classified by NESTORE. The more relevant features are S, Z, and Q at the six hours. The probabilities for the majority of these features exceed the threshold indicating that these features voted for the classification of this cluster as Type A and a strong aftershock with magnitude $\geq$ 3.9 was correctly expected to happen within a circular region with of radius R = 19 kilometers, in the 25 days after the o-mainshock. The number of clusters considered in this analysis is too small to allow a fully robust statistical evaluation. Nevertheless, the method's performance is consistent with the testing phase: the Type-A cluster was correctly classified (as were all Type-A clusters in the testing phase), while the only misclassifications occurred among the Type-B clusters, which also produced some false alarms during testing. A routine application of NESTORE to Greek seismicity would enable a more reliable performance assessment. The analysis of the misclassified Type-B clusters did not reveal any region-specific characteristics. In Anyfadi et al. (2023), the two misclassified Type-B clusters were located in eastern Crete and near the Anatolian peninsula coast, respectively, far from the location of the B cluster misclassified by the NRT algorithm.

5. Discussion and conclusions

In this paper, we have shown the performance of the NESTORE algorithm in classifying seismic clusters based on the characteristics of the first hours of seismicity after the o-mainshock. NESTORE is based on

a set of features extracted from seismic catalogues. It assumes that type A clusters (those with the strongest aftershocks) have large values of the features. In contrast, type B clusters typically show smaller values. The classification is based on threshold values for the features determined in the training phase. In all analysed regions, feature S, which refers to the normalized cumulative source area, has shown good results shortly after the o-mainshock (6 hours).

The capability of the S feature, in discriminating Type A and B clusters in most datasets for a short time after the mainshock may be interpreted from the physical point of view. Similarly to the analysis by Smirnov and Petruchov (2025) on precursors of strong earthquakes, we can state that, since the value of the normalised cumulative source area S is obtained from the aftershock magnitude and, from a physical perspective, the size of the sources is related to the size of lithospheric heterogeneity in fracturing (Scholz, 2019), the dimensional distribution of heterogeneities plays a crucial role in in determining the distribution of aftershock magnitudes (Aki, 1981). The development of fracturing and the subsequent stress redistribution lead to the widening of cracks as they merge. The tendency of cracks to coalesce into larger cracks, leading to the development of strong aftershocks, depends on the state of fracturing of the medium, the stress field, the orientation of cracks relative to the stress field, and the presence of fluids, and varies in time and space. Clusters in which this tendency is most pronounced are those where strong aftershocks (high S), with magnitudes comparable to that of the mainshock, are most likely to occur (type A clusters). This result is independent of the analyzed region. Clusters of type A, on the other hand, are also the ones characterized by strong fluctuations of S (as shown by SLCum and SLcum2) and higher variation of magnitude from event to event (as shown by Vm). This shift can interpreted as a manifestation of instability within the nonlinear system of earthquake-generating faults (Vorobieva, 1999), consistent with observations preceding major earthquakes and stronger events within seismic clusters (Keilis-Borok and Rotwain, 1990; Keilis-Borok and Kossobokov, 1990; Vorobieva and Panza, 1993).

From the machine learning point of view, the variability in feature performance across seismotectonic regimes highlights an important point: including a variety of features during training helps the model to adapt to regional differences. Some features show different performance depending on the analyzed area: the feature Q, referring to the cumulative radiated energy, works well in Greece, Italy and NE Italy-W

Slovenia, but not in California and Japan; the feature N_2, based on the earthquake number, gives good results in California, Italy and NE Italy-W Slovenia but not in Greece and Japan.

Overall, NESTORE correctly classified between 66 and 100% of type A clusters, and between 90 and 100% of type B clusters. The Precision, corresponding to the percentage of clusters classified as type A that actually were type A, ranged between 75% and 100%, depending on the class imbalance (lower precision if type B clusters are much more than type A clusters). Most of these results are obtained within the first 6-12 hours or at most within one day after the o-mainshock. Therefore, the method shows a great potential for application in seismic risk mitigation.

A recent and interesting result is that A and B clusters differ not only in terms of the strongest aftershock magnitude, but also in terms of the characteristics of the entire cluster, such as the cumulative seismic moment, duration and number of earthquakes. The analyses for Italy, NE Italy-W Slovenia and Japan have shown that the type A clusters have higher values for seismic moment, duration and number of earthquakes than the type B clusters with the same o-mainshock magnitude. Although the clusters in Italy and Japan depend on different seismotectonic contexts, seismic network characteristics, clustering laws and magnitude scales, it is interesting to note that to a first approximation, the different behaviour between type A and B clusters with respect to the three analysed characteristics is the same. The results on these three characteristics of seismicity provide shortly after the o-mainshock further information on how the ongoing cluster will behave.

Another interesting outcome of NESTORE is its capability of estimating feature thresholds robust enough to allow class forecasting in a whole region, even when multiple and diverse seismotectonic regimes coexist. The next step in our research investigation will be understanding whether the different values of the threshold from region to region are related to some characteristics of the seismicity. We therefore compared it with the geometric mean of the annual seismic rate that we found by analyzing the same catalogues. Recently, van der Elst & Page (2023) proposed a new method to estimate the seismic rate in the presence of incomplete data. This method, called a-positive (a+), is based on measuring the interevent time interval Δt_i, not between all earthquakes, as in the standard definition above, but only between pairs of earthquakes where the second event has a larger magnitude than the first. Specifically, the difference in magnitude between the two earthquakes in the pair must exceed a threshold value dM_{th}. By rescaling Δt_i with $10^{b(m_i+dM_{th})}$, the expected seismic rate can be estimated as if the catalog were complete.

Region	Geometric mean a+
Greece	$2.767282 \cdot 10^6$
Italy	$3.727444 \cdot 10^5$
Japan	$1.058114 \cdot 10^6$
California	$4.393627 \cdot 10^5$
NE Italy-W Slovenia	$3.128294 \cdot 10^3$

Table 4: Geometric mean of annual seismic rate a+

Table 4 shows the geometric mean for the parameter a+. We used the geometric mean because the distribution of the a+ values is very skewed and long-tailed, due to the considerably heterogeneous and clustered nature of seismicity. Greece and Japan have the highest productivity value; Italy and California are in the middle range, while NE Italy-W Slovenia has the lowest values. We hypothesise that the threshold values of the features may be related to the seismic rate. When the rate is higher, both the A and B clusters show higher values for the features and thus higher thresholds while, conversely, a lower rate leads to lower thresholds for both the A and B clusters.

While the relationship between the seismicity rate of the whole catalogue and e.g. the cumulative radiated energy or the cumulative source area of clusters is not obvious, the value of a+ in the whole catalogue can be more easily related to the number of events with a magnitude ≥Mm-2 in the clusters. The seismicity rate simply behaves the same way in the whole catalogue and in the clusters, and regions with higher a+ are also those with a higher number of events with magnitude ≥Mm-2 in both the A and B clusters. As shown in Section 4.3, Japan and Italy are characterised by a higher number of events with M≥Mm-2 for the A class compared to NE Italy-W Slovenia. This difference is also reflected in the threshold on N_2, which only covers the first hours of the cluster and is smaller for NE Italy-W Slovenia than in Italy; for Japan, the decision tree for N_2 does not converge.

Understanding how differences in fault geometry, slip rates and tectonic loading can influence seismic patterns is essential for the future improvement of machine learning methods such as NESTORE, which

aims to forecast strong aftershocks in different tectonic settings. Trugman & Ben-Zion (2023) conducted a comprehensive analysis of the productivity of earthquake sequences in California and Nevada using a 40-year seismicity catalogue and nearest-neighbour clustering. They showed that productivity variations are strongly related to geophysical parameters such as heat flow, fault complexity and deformation velocity. Highly productive sequences are found in areas such as the Walker Lane, lower productivity ones along the San Andreas Fault. Using XGBoost and SHAP, they showed how these physical conditions influence the clustering and triggering potential of earthquakes.

Their results provide a useful framework for interpreting the classification of A and B-type clusters in NESTORE. Since high heat flow, high fault density and high complexity are associated with high productivity, these parameters could help explain why certain clusters evolve into A-type clusters while others remain B-type.

Both Gentili and Di Giovambattista (2022) and Trugman and Ben-Zion (2023) use interpretable machine learning approaches and focus on seismicity in California seismicity, showing potential from the combination of seismic and geophysical features to improve NESTORE forecasts.

NESTORE is still under development and several studies are in progress, such as the application to New Zealand (Caravella and Gentili, 2025) and the use of new features in improved catalogues such as RAMONES, which includes also the energy and seismic moment (Brondi et al., 2024). Furthermore, routine testing has been conducted in Italy and in the northeastern Italy–western Slovenia region since 2021. The analysis is based on the real-time version of the catalogues, which may have reduced accuracy in event location and detection performance. Although the proposed results require validation on a larger test set, they show performance levels consistent with those achieved during the testing phase, confirming that NESTORE also performs well on unrevised catalogues.

Newer performance assessments are planned where the best performance interval for NESTORE, as shown in Fig. 2, is estimated not only in the predefined test set but by a k-fold approach. This approach could be particularly important for the NRT module, where we apply NESTORE to new clusters after training with both the old training set and the old test set, while the window in which performances are considered optimal is estimated based on the old test set only.

6. Author contributions

The authors contributed to the results in the corresponding previous publications on NESTORE, without their work, this paper would not have been written. In this paper, the work has been subdivided in the following way.

Stefania Gentili: Conceptualization, Methodology, Software, Validation, Formal analysis, Investigation, Resources, Data Curation, Writing - Original Draft, Writing - Review & Editing, Visualization, Supervision, Project administration, Funding acquisition; **Piero Brondi:** Software, Validation, Formal analysis, Investigation, Resources, Data Curation, Writing - Original Draft, Writing - Review & Editing; **Giuseppe Davide Chiappetta:** Software, Validation, Formal analysis, Investigation, Data Curation, Writing - Original Draft, Writing - Review & Editing, Visualization; **Giuseppe Petrillo:** Software, Validation, Formal analysis, Investigation, Writing - Original Draft, Writing - Review & Editing; **Jiancang Zhuang:** Methodology, Software, Resources, Writing - Review & Editing, Supervision, Project administration, Funding acquisition; **Eleni-Apostolia Anyfadi** Validation, Formal analysis, Investigation, Data Curation, Writing - Original Draft, Writing - Review & Editing; **Filippos Vallianatos** Writing - Review & Editing, Supervision, Project administration, Funding acquisition; **Letizia Caravella** Writing - Original Draft, Writing - Review & Editing; **Enrico Magrin** Software; **Paolo Comelli** Software; **Rita Di Giovambattista** Conceptualization, Methodology, Validation, Formal analysis, Investigation, Resources, Writing - Original Draft, Writing - Review & Editing,

7. Acknowledgments

Following the presentation at the recent GNGTS conference (Gentili et al., 2025), the work was recognized by the conveners as worthy of publication in this special issue of the Bulletin of Geophysics and Oceanography (BGO).

This work is Co-funded within the RETURN Extended Partnership and received funding from the European Union Next-GenerationEU (National Recovery and Resilience Plan - NRRP, Mission 4, Component 2, Investment 1.3 – D.D. 1243 2/8/2022, PE0000005) and by the grant “Progetto INGV Pianeta Dinamico: Near real-time results of Physical and Statistical Seismology for earthquakes observations, modelling and forecasting (NEMESIS)” - code CUP D53J19000170001 - funded by Italian

Ministry MIUR (“Fondo Finalizzato al rilancio degli investimenti delle amministrazioni centrali dello Stato e allo sviluppo del Paese”, legge 145/2018).
G.P. would like to acknowledge the Earth Observatory of Singapore (EOS), and the Singapore Ministry of Education Tier 3b project “Investigating Volcano and Earthquake Science and Technology (InVEST)”. G.P. and J.Z. are also partially supported by the Japan Ministry of Education, Culture, Sports, Science and Technology (MEXT) project for seismology Toward Research innovation with data of earthquakes (STAR-E), Grant Number JPJ010217. Another project, actually ended, strongly contributed to the results used in this analysis: the Bilateral project Italy–Japan funded by a grant from the Italian Ministry of Foreign Affairs and International Cooperation was pivotal for NESTORE development. E-A A was partially supported by the Erasmus+ programme of the European Union (EU).
Map figures have been realized using QGIS (http://www.qgis.org), while other analyses have been performed using ZMAP (http://www.seismo.ethz.ch/en/research-and-teaching/products-software/software/ZMAP). For The NESTOREv1.0 toolbox is available for free download from GitHub at the address https://github.com/StefaniaGentili/NESTORE and its reproducibility package is available on Zenodo https://zenodo.org/account/settings/github/repository/StefaniaGentili/NESTORE.

8. References

ANSS Comprehensive Earthquake Catalog (ComCat) https://earthquake.usgs.gov/earthquakes/search/

Aki, K.; 1981 Probabilistic synthesis of precursory phenomena in earthquake prediction, in Earthquake Prediction: An International Review, Washington: Amer. Geophys. Union, pp. 556–574.

Alatza S.; 2013: *Geodetic determination of tectonic displacements in Chalkidiki*. (Bachelor's thesis), National Technical University of Athens School of Surveying and Surveying Engineering.

Ambraseys N.N., Jackson J.A.; 1997: *Seismicity and strain in the Gulf of Corinth (Greece) since 1694*. J. Earthq. Eng., **1**, 433–474, DOI:10.1080/13632469708962374.

Anyfadi E.-A., Gentili S., Brondi P., Vallianatos F.; 2023: *Forecasting Strong Subsequent Earthquakes in Greece with the Machine Learning Algorithm NESTORE*. Entropy, **25**(5), DOI:10.3390/e25050797.

Anyfadi E.-A.; 2023: *Forecasting Strong Aftershocks in Greek Earthquake Clusters Using the NESTORE Machine Learning Algorithm*. Master's Thesis, Hellenic Republic National and Kapodistrian University of Athens, Department of Geology and Geoenvironment, Sector of Geophysics and Geothermy.

Argus D.F., Gordon R.G., DeMets C.; 2011: *Geologically current motion of 56 plates relative to the no-net-rotation reference frame*. Geochem. Geophys. Geosyst., **12**(11), DOI:10.1029/2011GC003751.

Azzara R., Basili A., Beranzoli L., Chiarabba C., Di Giovambattista R., Selvaggi G.; 1993: *The seismic sequence of Potenza (May 1990)*. Ann. Geofis., **36**, 237–243.

Bailer-Jones, C. A. L., Smith, K.; 2011: *Combining probabilities* GAIA-C8-TN-MPIA-CBJ-053 https://www.mpia.de/3432751/probcomb_TN.pdf.

Bressan G., Barnaba C., Magrin A., Rossi G.; 2018: *A study on off-fault aftershock pattern at N-Adria microplate*. J. Seismol., **22**, 863–881.

Bressan G., Bragato P.L., Venturini C.; 2003: *Stress and strain tensors based on focal mechanisms in the seismotectonic framework of the Friuli-Venezia Giulia region (Northeastern Italy)*. Bull. Seismol. Soc. Am., **93**, 1280–1297.

Bressan G., Gentile G.F., Perniola B., Urban S.; 2009: *The 1998 and 2004 Bovec-Krn (Slovenia) seismic sequences: aftershock pattern, focal mechanisms and static stress changes*. Geophys. J. Int., **179**, 231–253.

Bressan G., Gentile G.F., Tondi R., de Franco R., Urban S.; 2012: *Sequential Integrated Inversion of Tomographic Images and Gravity Data: An Application to the Friuli Area (North-Eastern Italy)*. Boll. Geofis. Teor. Appl., **53**, 191–212.

Bressan G., Ponton M., Rossi G., Urban S.; 2016: *Spatial organization of seismicity and fracture pattern in NE-Italy and W-Slovenia*. J. Seismol., **20**, 511–534.

Brondi P., Gentili S., Di Giovambattista R.; 2025: *Forecasting strong subsequent events in the Italian territory: a National and Regional application for NESTOREv1.0*. Natural Hazards, **121**, 3499–3531, DOI:10.1007/s11069-024-06913-6.

Brondi P., Gentili S., Picozzi M., Spallarossa D., Di Giovambattista R.; 2024: *Characterizing clusters with strong subsequent events in Central Italy using RAMONES*. EGU General Assembly 2024, Vienna, Austria, 14–19 April 2024, EGU24-6346, DOI:10.5194/egusphere-egu24-6346.

Brondi P., Snidarcig A., Bernardi P., Bragato P.L., Di Bartolomeo P.; 2024b: *Bollettino della Rete Sismometrica dell'Italia Nord Orientale (RSINO)*. [Data set]. Istituto Nazionale di Oceanografia e di Geofisica Sperimentale - OGS, DOI:10.13120/w1vp-b578.

Brondi P., Snidarcig A., Di Bartolomeo P., Magrin A., Barnaba C., Poggi V., Pettenati F., Romanelli M., Rebez A., Moratto L., Sandron D., Plasencia M.,Pesaresi D., Compagno A., Del Negro E., Comelli P., Magrin E., Zuliani D., Bertoni M., Fabris P., and Bernardi P.; 2025b: *Bollettino della Rete Sismometrica dell'Italia Nord Orientale (RSINO), Anno 2023* [Data set]. Istituto Nazionale di Oceanografia e di Geofisica Sperimentale - OGS. DOI: 10.13120/m4pk-nd81

Caravella L. and Gentili S.; 2025: *Forecasting strong subsequent aftershocks in New Zealand: preliminary results*. Applied Statistics 2025, September 21–23, Koper/Capodistria, Slovenia.

Calderoni G., Rovelli A., Di Giovambattista R.; 2017: *Rupture directivity of the strongest 2016–2017 Central Italy earthquakes*. J. Geophys. Res., **122**, 9118–9131.

Caputo R.; 1995: *Inference of a seismic gap from geological data: Thessaly (Central Greece) as a case study*. Ann. Geophys., **38**, 1–19.

Caputo R. and Pavlides, S.; 1993: *Late Cainozoic Geodynamic Evolution of Thessaly and Surroundings (Central-Northern Greece)*. Tectonophysics, **223**, 339–362, DOI:10.1016/0040-1951(93)90144-9.

Chiarabba C., De Gori P., Speranza F.; 2008: *The southern Tyrrhenian subduction zone: deep geometry, magmatism and Plio-Pleistocene evolution*. Earth Planet. Sci. Lett., **268**(3–4), 408–423.

Delibasis N., Ziazia M., Voulgaris N., Papadopoulos T., Stavrakakis G., Papanastassiou D., Drakatos G.; 1999: *Microseismic activity and seismotectonics of Heraklion area (central Crete Island, Greece)*. Tectonophysics, **308**(1–2), 237–248.

DeMets C., Gordon R.G., Argus D.F.; 2010: *Geologically current plate motions*. Geophys. J. Int., **181**(1), 1–80, DOI:10.1111/j.1365-246X.2009.04491.x.

Devoti R., Riguzzi F., Cuffaro M., Doglioni C.; 2008: *New GPS constraints on the kinematics of the Apennines subduction*. Earth Planet. Sci. Lett., **273**(1–2), 163–174, DOI:10.1016/j.epsl.2008.06.031.

DeVries P.M.R., Viégas F., Wattenberg M. et al.; 2018: *Deep learning of aftershock patterns following large earthquakes*. Nature, **560**, 632–634, DOI:10.1038/s41586-018-0438-y.

Dimitriadis, I., Papazachos, C., Panagiotopoulos, D., Hatzidimitriou, P., Bohnhoff, M., Rische, M., Meier, T.; 2010: *P and S velocity structures of the Santorini-Coloumbo volcanic system (Aegean Sea, Greece) obtained by non-linear inversion of travel times and its tectonic implications* J. Volcanol. Geotherm. Res., **195**(1), 13-30, DOI: 10.1016/j.jvolgeores.2010.05.013

Doglioni C.; 1991: *A proposal of kinematic modelling for W-dipping subductions – possible applications to the Tyrrhenian-Apennines system*. Terra Nova, **3**, 423–434.

Doglioni C.; 1995: *Geological remarks on the relationships between extension and convergent geodynamic settings*. Tectonophysics, **252**, 253–268.

Doglioni C., Carminati E., Cuffaro M., Scrocca D.; 2007: *Subduction kinematics and dynamic constraints*. Earth-Sci. Rev., **83**(3–4), 125–175.

Gardner J.K. and Knopoff L.; 1974: *Is the sequence of earthquakes in Southern California, with aftershocks removed, Poissonian?* Bull. Seismol. Soc. Am., **64**(5), 1363–1367, DOI:10.1785/BSSA0640051363.

Gkarlaouni, C., Papadimitriou, E., Karakostas, V., Kilias, A. and Lasocki, S., 2015: *Fault population recognition through microseismicity in Mygdonia region (northern Greece)*. Bollettino di Geofisica Teorica ed Applicata, **56**(3).

Gentili S. and Bressan G.; 2008: *The partitioning of radiated energy and the largest aftershock of seismic sequences occurred in the northeastern Italy and western Slovenia*. J. Seismol., **12**, 343–354, DOI:10.1007/s10950-007-9075-x.

Gentili S. and Di Giovambattista R.; 2017: *Pattern recognition approach to the subsequent event of damaging earthquakes in Italy*. Phys. Earth Planet. Inter., **266**, 1–17, DOI:10.1016/j.pepi.2017.02.011.

Gentili S. and Di Giovambattista R.; 2020: *Forecasting strong aftershocks in earthquake clusters from northeastern Italy and western Slovenia*. Phys. Earth Planet. Inter., **303**, DOI:10.1016/j.pepi.2020.106483.

Gentili S. and Di Giovambattista R.; 2022: *Forecasting strong subsequent earthquakes in California clusters by machine learning*. Phys. Earth Planet. Inter., **327**, DOI:10.1016/j.pepi.2022.106879.

Gentili S. and Gentile G.F.; 2015: *High frequency attenuation k parameter and QS 3D model for south-eastern Alps and north-western Dinarides*. Boll. Geofis. Teor. Appl., **56**, 383–406.

Gentili S. and Franceschina G.; 2011: *High frequency attenuation of shear waves in the southeastern Alps and northern Dinarides*. Geophys. J. Int., **185**, 1393–1416.

Gentili S., Brondi P., Di Giovambattista R.; 2023: *NESTOREv1.0: A MATLAB Package for Strong Forthcoming Earthquake Forecasting*. Seismol. Res. Lett., **94**(4), 2003–2013, DOI:10.1785/0220220327.

Gentili S., Brondi P., Di Giovambattista R.; 2023b: *Machine Learning for Forecasting Strong Aftershocks in California: the NESTOREv1.0 Application*. AGU23, San Francisco, CA, 11–15 December 2023. Bibcode: 2023AGUFM.S33I0499G.

Gentili S., Brondi P., Rossi G., Sugan M., Petrillo G., Zhuang J., Campanella S.; 2024: *Seismic clusters and fluids diffusion: a lesson from the 2018 Molise (Southern Italy) earthquake sequence*. Earth Planets Space, **76**, 157, DOI:10.1186/s40623-024-02096-3.

Gentili S., Chiappetta G.D., Petrillo G., Brondi P., Zhuang J.; 2025: *Forecasting strong subsequent earthquakes in Japan using an improved version of NESTORE machine learning algorithm*. Geoscience Frontiers, **16**(3), DOI:10.1016/j.gsf.2025.102016.

Godano C., Petrillo G., Tramelli A., Convertito V.; 2025: *The b b-Value Tomography of the Calabrian Arc*. Earth Space Sci., **12**(6), e2024EA004065.

Hauksson E. and Shearer P.M.; 2005: *Southern California hypocenter relocation with waveform cross-correlation, part 1: Results using the double-difference method*. Bull. Seismol. Soc. Am., **95**(3), 896–903, DOI:10.1785/0120040167.

Hutton K., Woessner J., Hauksson E.; 2010: *Earthquake monitoring in Southern California for seventy-seven years (1932–2008)*. Bull. Seismol. Soc. Am., **100**, 423–446.

ISIDe Working Group; 2007: *Italian Seismological Instrumental and Parametric Database (ISIDe)*. Istituto Nazionale di Geofisica e Vulcanologia (INGV), DOI:10.13127/ISIDE.

Japan Meteorological Agency; 2024: *The seismological bulletin of Japan*. https://www.data.jma.go.jp/svd/eqev/data/bulletin/index_e.html

Kanamori H.; 1972: *Tectonic implications of the 1944 Tonankai and the 1946 Nankaido earthquakes*. Phys. Earth Planet. Inter., **5**, 129–139, DOI:10.1016/0031-9201(72)90082-9.

Karimzadeh S., Matsuoka M., Kuang J., Ge L.; 2019: *Spatial Prediction of Aftershocks Triggered by a Major Earthquake: A Binary Machine Learning Perspective*. ISPRS Int. J. Geo-Inf., **8**, 462, DOI:10.3390/ijgi8100462.

Keilis-Borok, V.I., Kossobokov, V.G., 1990: *Premonitory activa- tion of earthquake flow: algorithm M8.* Phys. Earth Planet. Inter. **61**, 73–83.

Keilis-Borok, V.I., Rotwain, I.M., 1990: *Diagnosis of time of increased probability of large earthquakes in different regions of the world: algorithm CN.* Phys. Earth Planet. Inter. **61**, 57–72.

Koukouvelas I.K., Kokkalas S., Xypolias P.; 2010: *Surface deformation during the Mw 6.4 (8 June 2008) Movri Mountain earthquake in the Peloponnese, and its implications for the seismotectonics of western Greece*. Int. Geol. Rev., **52**(2–3), 249–268.

Lay T.; 2018: *A review of the rupture characteristics of the 2011 Tohoku-oki Mw 9.1 earthquake*. Tectonophysics, **733**, 4–36, DOI:10.1016/j.tecto.2017.09.022.

Le Pichon, X., Chamot-Rooke, N., Lallemant, S., Noomen, R., Veis, G.: 1995. *Geodetic determination of the kinematics of Central Greece with respect to Europe: implications for eastern Mediterranean tectonics* J. Geophys. Res., **100**(B7), 12,675-12,690, DOI:10.1029/95JB00317

Lippiello E. and Petrillo G.; 2024: *b-more-incomplete and b-more-positive: Insights on a robust estimator of magnitude distribution*. J. Geophys. Res.: Solid Earth, **129**(2), e2023JB027849.

Liu B., Wen H., Di M., Huang J., Liao M., Yu J., Xiang Y.; 2024: *Mapping and interpretability of aftershock hazards using hybrid machine learning algorithms*. J. Rock Mech. Geotech. Eng.

Lolli B. and Gasperini P.; 2003: *Aftershocks hazard in Italy Part I: Estimation of time-magnitude distribution model parameters and computation of probabilities of occurrence*. J. Seismol., **7**(2), 235–257.

Lolli B. and Gasperini P.; 2006: *Comparing different models of aftershock rate decay: the role of catalog incompleteness in the first times after mainshock*. Tectonophysics, **423**, 43–59, DOI:10.1016/j.tecto.2006.03.025.

Malinverno A. and Ryan W.B.F.; 1986: *Extension in the Tyrrhenian Sea and shortening in the Apennines as a result of arc migration driven by sinking of the lithosphere*. Tectonics, **5**, 227–245.

McClusky, S., Balassanian, S., Barka, A., Demir, C., Ergintav, S., Georgiev, I., Gurkan, O., Hamburger, M., Hurst, K., Kahle, H., et al. 2000: Global *Positioning System constraints on plate kinematics and dynamics in the eastern Mediterranean and Caucasus. J. Geophys. Res.*, **105**, 5695–5719.

McKenzie, D.; 1978: *Active tectonics of the Alpine-Himalayan belt: The Aegean Sea and surrounding regions*. Geophys. J. R. Astron. Soc., **55**, 217–254 .

Mignan A. and Broccardo M.; 2020: *Neural network applications in earthquake prediction (1994–2019): meta-analytic and statistical insights on their limitations*. Seismol. Res. Lett.

Milano G. and Di Giovambattista R.; 2011: *Seismicity at the border between Central and Southern Apennines (Italy): re-evaluation of the early 1984 instrumental earthquake*. Tectonophysics, **499**, 92–104, DOI:10.1016/j.tecto.2010.12.008.

Miller S.A., Collettini C., Chiaraluce L., Cocco M., Barchi M., Kaus B.J.P.; 2004: *Aftershocks driven by a high-pressure CO2 source at depth*. Nature, **427**, 724–727.

NCEDC 2014: Northern California Earthquake Data Center. UC Berkeley Seismological Laboratory. Dataset. doi:10.7932/NCEDC.

Ogata Y.; 1988: *Statistical models for earthquake occurrences and residual analysis for point processes*. J. Am. Stat. Assoc., **83**(401), 9–27, DOI:10.2307/2288914.

Ogata Y. and Zhuang J.; 2006: *Space-time ETAS model and an improved extension*. Tectonophysics, **413**(1–2), 13–23, DOI:10.1016/j.tecto.2005.10.016.

Papazachos, B., Karakostas, V., Papazachos, C., Scordilis, E.; 2000. *The geometry of the Wadati–Benioff zone and lithospheric kinematics in the Hellenic arc*. Tectonophysics, **319**(4), 275-300, DOI:10.1016/S0040-1951(99)00299-1

Petrillo G. and Zhuang J.; 2022: *The debate on the earthquake magnitude correlations: a meta-analysis*. Sci. Rep., **12**(1), 20683.

Petrillo G. and Zhuang J.; 2023: *Verifying the magnitude dependence in earthquake occurrence*. Phys. Rev. Lett., **131**(15), 154101.

Picozzi M., Abdi F., Barnaba C., Bertoni M., Bragato P.L., Brondi P., Caravella L., Capotosti G., Cataldi L., Comelli P., Compagno A., Chiappetta G.D., Gentili S., Fabris P., Fangqing D., Magrin A., Moratto L., Pesaresi D., Peruzza L., Poggi V., Romano M.A., Rossi G., Sandron D., Santulin M., Saraò A., Spallarossa D., Sugan M., Zuccolo E.; 2025: *Rapporto di sintesi sul Terremoto di Raveo ML 3.9 del 12 Gennaio 2025 (Udine)*, DOI:10.5281/zenodo.15168324.

Polonia A., Torelli L., Artoni A., Carlini M., Faccenna C., Ferranti L., Gasperini L., Govers R., Klaeschen D., Monaco C., Neri G., Nijholt N., Orecchio B., Wortel R.; 2016: *The Ionian and Alfeo–Etna fault zones: New segments of an evolving plate boundary in the central Mediterranean Sea?* Tectonophysics, **675**, 69–90, DOI:10.1016/j.tecto.2016.03.016.

Reilinger, R., McClusky, S., Paradisis, D., Ergintav, S., Vernant.; 2010; *Geodetic constraints on the tectonic evolution of the Aegean region and strain accumulation along the Hellenic subduction zone* Tectonophysics, **488**, 22-30, DOI: 10.1016/j.tecto.2009.05.027

Rousseeuw P.J. and Hubert M.; 2011: *Robust statistics for outlier detection*. Wiley Interdiscip. Rev.: Data Mining Knowl. Discov., **1**(1), 73–79, DOI:10.1002/widm.2.

Sakellariou D., Lykousis V., Alexandri S., Kaberi H., Rousakis G., Nomikou P., Georgiou P., Ballas D.; 2007: *Faulting, seismic-stratigraphic architecture and Late Quaternary evolution of the Gulf of Alkyonides Basin–East Gulf of Corinth, Central Greece*. Basin Res., **19**, 273–295, DOI:10.1111/j.1365-2117.2007.00322.x.

SCEDC; 2013: *Southern California Earthquake Center*. Caltech. Dataset, DOI:10.7909/C3WD3xH1.

Schimmenti V.M., Petrillo G., Rosso A., Landes F.P.; 2024: *Assessing the predictive power of GPS-based ground deformation data for aftershock forecasting*. Seismol. Res. Lett., **95**(6), 3243–3249, DOI:10.1785/0220240008.

Scholz, C.H.; 2019: *The Mechanics of Earthquakes and Faulting*, Cambridge Univ. Press.

Smirnov V. B., Petruchov A. A.; 2025: *On the Relationship between RTL and b-Value Anomalies of Seismicity.* Izvestiya, Physics of the Solid Earth, 2025, **61**(4), 539–552. DOI:10.1134/S1069351325700545

Snidarcig A., Bernardi P., Bragato P.L., Di Bartolomeo P., Garbin M., Urban S.; 2020: *Bollettino della rete sismometrica dell'Italia Nord Orientale (RSINO)*. Istituto Nazionale Di Oceanografia e Di Geofisica Sperimentale - OGS, DOI: 10.13120/108b8d94-361a-45f3-8195-fc4e8f73d264.

Snidarcig A., Bernardi P., Bragato P.L., Di Bartolomeo P., Garbin M., Urban S.; 2021: *Bollettino della Rete Sismometrica dell'Italia Nord Orientale (RSINO)*. [Data set]. Istituto Nazionale di Oceanografia e di Geofisica Sperimentale - OGS, DOI:10.13120/8b252b09-314f-456f-812a-b05268ecd001.

Sweets J.A., Dawes R.M., Monahan J.; 2000: *Better decisions through science*. Sci. Am., **283**, 82–87.

Spassiani I., Gentili S., Console R., Murru M., Taroni M., Falcone G.; 2025: *Reconciling the irreconcilable: window-based versus stochastic declustering algorithms*. Geophys. J. Int., **240**(2), 1009–1027, DOI:10.1093/gji/ggae425.

Stockman S., Lawson D.J., Werner M.J.; 2023: *Forecasting the 2016–2017 Central Apennines earthquake sequence with a neural point process*. Earth's Future, **11**, e2023EF003777, DOI:10.1029/2023EF003777.

Totaro C., Orecchio B., Presti D., Scolaro S., Neri G.; 2016: *Seismogenic stress field estimation in the Calabrian Arc region (south Italy) from a Bayesian approach*. Geophys. Res. Lett., **43**, 8960–8969, DOI:10.1002/2016GL070107.

Trugman D.T. and Ben-Zion Y.; 2023: *Coherent spatial variations in the productivity of earthquake sequences in California and Nevada*. Seism. Rec., **3**(4), 322–331, DOI:10.1785/0320230039.

Uhrhammer R.A.; 1986: *Characteristics of northern and central California seismicity*. Earthquake Notes, **57**, 21–37.

Vallianatos F., Michas G., Hloupis G.; 2021: *Seismicity Patterns Prior to the Thessaly (Mw6.3) Strong Earthquake on 3 March 2021 in Terms of Multiresolution Wavelets and Natural Time Analysis*. Geosciences, **11**(9), 379, DOI:10.3390/geosciences11090379.

Vallianatos F., Karakonstantis A., Michas G., Pavlou K., Kouli M., Sakkas V.; 2022: *On the Patterns and Scaling Properties of the 2021–2022 Arkalochori Earthquake Sequence (Central Crete, Greece) Based on Seismological, Geophysical and Satellite Observations*. Appl. Sci., **12**(15), 7716, DOI:10.3390/app12157716.

van der Elst N.J. and Page M.T.; 2023: *a-positive: A robust estimator of the earthquake rate in incomplete or saturated catalogs*. J. Geophys. Res.: Solid Earth, **128**(10), e2023JB027089, DOI:10.1029/2023JB027089.

Vorobieva, I.A.; 1999: *Prediction of a subsequent large earthquake*. Phys. Earth Planet. Inter. **111**, 197–206.

Vorobieva, I.A., Panza, G.F.; 1993: *Prediction of the occurrence of related strong earthquakes in Italy.* PAGEOPH **141** (1), 25–41. DOI:10.1007/BF00876232.Wang M., Shen J., Pan Z.A., Han D.L.; 2019: *An improved supported vector regression algorithm with application to predict aftershocks*. J. Seismol., **23**(5), 983–993.

Wu J., Suppe J., Lu R., Kanda R.; 2016: *Philippine Sea and East Asian plate tectonics since 52 Ma constrained by new subducted slab reconstruction methods*. J. Geophys. Res.: Solid Earth, **121**(6), 4670–4741, DOI:10.1002/2016JB012923.

Zechar, J.D.; 2010: *Evaluating earthquake predictions and earthquake forecasts: a guide for students and new researchers*, Community Online Resource for Statistical Seismicity Analysis, doi:10.5078/corssa-77337879. Available at http://www.corssa.org.

Zhao S., Wang H., Xue Y. et al.; 2022: *What are more important for aftershock spatial distribution prediction, features, or models? A case study in China*. J. Seismol., **26**, 181–196, DOI:10.1007/s10950-021-10044-x.

Zhuang J., Ogata Y., Vere-Jones D.; 2002: *Stochastic Declustering of Space-Time Earthquake Occurrences*. J. Am. Stat. Assoc., **97**(458), 369–380, DOI:10.1198/016214502760046925.

9. Figure captions

Fig. 1: Analyzed areas in past NESTORE applications.

Fig. 2: Performances of NESTORE in different regions.

Fig. 3: Thresholds for each feature and time period (when available) for the analyzed regions.

Fig. 4: Near Real Time module performances on INGV catalogue.

Fig. 5: Near Real Time module performances on OGS catalogue.

Fig. 6: Near Real Time module performances on AUTH catalogue.

10. Table captions

Table 1: Adopted catalogues in different regions and time period for which they are used.

Table 2: Training set and Test set cardinality for the analysed areas.

Table 3: Values of α for the different regions

Table 4: Geometric mean of a+

Appendix

Online NRT software and web page on OGS data

The OGS automatic seismic monitoring system managed by its department CRS (Seismological Research Centre) performs several real-time procedures as parts of its 24/7 monitoring activity, including localising events, estimating their magnitude, and forwarding warnings to civil protection authorities. We integrated the NESTORE Near Real-Time (NRT) module among these processes. To support this functionality, a dedicated server has been set up that continuously monitors for new events that exceed the magnitude threshold and executes the NRT module. This module, like the rest of the NESTORE codebase, is written in MATLAB. For our purpose, it is wrapped in a shell script that handles the interaction with the Linux operating system. When an event is detected, the server first evaluates whether the event fulfills the conditions 1 and 2 for the NESTORE NRT analysis.

If these criteria are satisfied, the system automatically prepares the required environment (generating input files and directory structures) and launches the NRT analysis in a temporary workspace (see Fig. A1). NESTORE stores as potential aftershocks all events that occur within the following 6 hours and within a radius that depends on Mm according to the window-based law defined in the training and testing (see section 3.2). If the magnitude of the strongest aftershock is greater than or equal to Mm−1, there are two possibilities:

1. If the magnitude is greater than Mm, the aftershock becomes the new operative mainshock, and the procedure restarts.

2. If the magnitude is lower than Mm, the cluster is already classified as type A and no further classification is performed.

This minor change to the original algorithm (the branch in point 1 was not present in the original algorithm) was added taking into account the low threshold (ML=3.7) for the o-mainshock in the region, to allow analysis even in cases where the mainshock is preceded by a small (e.g. ML=3.7 or similar) foreshock a few hours earlier by a small foreshock.

If in the first 6 hours after the mainshock the aftershocks have magnitudes lower than Mm−1, the seismic features are analyzed and the system calculates the probability that the cluster is of type A based on prior machine learning training. The output includes the forecasted cluster class, its probability, and the spatiotemporal window for the forecasting.

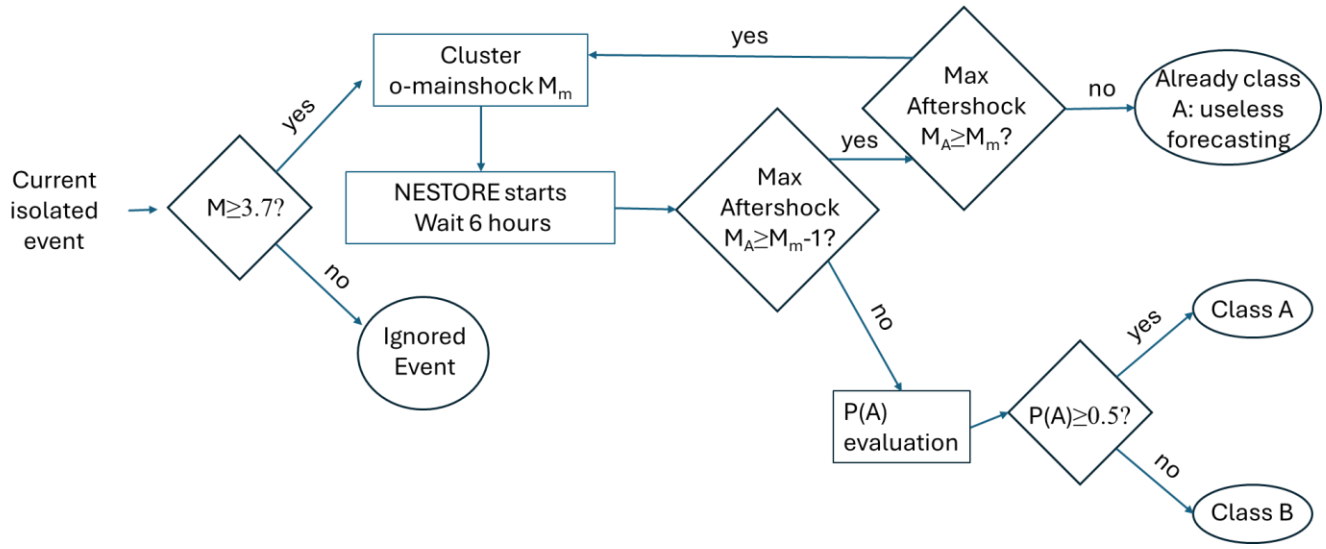

Fig. A1: Block diagram of the NRT algorithm

Since the best results of the test phase in the region were obtained for a period of 6 hours after the main o-mainshock, according to the NRT procedure the NRT performance should only be considered for 6 hours. In order to consider the possible future trainings on larger database which may show better results for longer time intervals, the procedure is performed for all the intervals for which we had a training, i.e. 6, 12 and 18 hours after the o-mainshock. The o-mainshock is kept unchanged for longer time intervals, to avoid confusion with the 6-hours analysis.

Since alerts are typically received by the NESTORE server within a few minutes after the event origin time, the automated pipeline is configured to wait for the minimum time window (6 hours) before querying the CRS server for the updated aftershock catalog (if available). This approach ensures that the analysis is based on the most up-to-date information (e.g. location, magnitude), which may have been refined by an operator in the meantime, and allows the system to deliver an informed classification (Type A or B). The final output is published at: https://nestore.crs.ogs.it. The site is under development and is password protected. At present, the algorithm has correctly processed two sequences in 2024 (see Fig. 5). On January 12, 2025 a ML 3.9 occurred close to the Raveo Village (Picozzi et al., 2025), followed by an event of magnitude ML=3.3in the first 6 hours after the mainshock. According to the procedure shown in the block diagram in Fig. A1, the cluster already turned out to be an A-type cluster in the first 6 hours, as the second event was not strong enough to become a new operative mainshock. The cluster did not require any further forecasting and was therefore ignored.